

Beyond MSE: Ordinal Cross-Entropy for Probabilistic Time Series Forecasting

Jieting Wang, Huimei Shi, Feijiang Li, Xiaolei Shang

¹Institute of Big Data Science and Industry, Shanxi University

²Key Laboratory of Evolutionary Science Intelligence of Shanxi Province, Taiyuan, China

Abstract

Time series forecasting is an important task that involves analyzing temporal dependencies and underlying patterns (such as trends, cyclicity, and seasonality) in historical data to predict future values or trends. Current deep learning-based forecasting models primarily employ Mean Squared Error (MSE) loss functions for regression modeling. Despite enabling direct value prediction, this method offers no uncertainty estimation and exhibits poor outlier robustness. To address these limitations, we propose OCE-TS, a novel ordinal classification approach for time series forecasting that replaces MSE with Ordinal Cross-Entropy (OCE) loss, preserving prediction order while quantifying uncertainty through probability output. Specifically, OCE-TS begins by discretizing observed values into ordered intervals and deriving their probabilities via a parametric distribution as supervision signals. Using a simple linear model, we then predict probability distributions for each timestep. The OCE loss is computed between the cumulative distributions of predicted and ground-truth probabilities, explicitly preserving ordinal relationships among forecasted values. Through theoretical analysis using influence functions, we establish that cross-entropy (CE) loss exhibits superior stability and outlier robustness compared to MSE loss. Empirically, we compared OCE-TS with five baseline models—Autoformer, DLinear, iTransformer, TimeXer, and TimeBridge—on seven public time series datasets. Using MSE and Mean Absolute Error (MAE) as evaluation metrics, the results demonstrate that OCE-TS consistently outperforms benchmark models. The code is publicly available at: <https://github.com/Shi-hm/OCE-TS>.

Introduction

Long-term time series forecasting plays a vital role in practical applications such as industrial monitoring, traffic management, and financial risk control. Traditional forecasting methods including Autoregressive Integrated Moving Average (ARIMA) (Box et al. 2015), Error-Trend-Seasonal (ETS) models (Hyndman et al. 2008), and Prophet (Taylor and Letham 2018) typically require manual feature engineering and make certain assumptions about data patterns.

Recent advances in deep learning have significantly improved time series forecasting performance (Li et al. 2019b).

Modern architectures can automatically learn complex temporal features and long-term dependencies, achieving state-of-the-art performance in various forecasting tasks (Lim et al. 2021). Particularly for long-term forecasting tasks, current research demonstrates that Transformer-based models (Zhou et al. 2021; Wu et al. 2021), modern Multilayer Perceptron (MLP) architectures (Zeng et al. 2023), and enhanced Long Short-Term Memory (LSTM) networks (Gruff et al. 2017) can all effectively extract multi-scale features from time series through end-to-end training. These developments have been further validated in comprehensive benchmarks (Zhou et al. 2022), establishing neural methods as the new paradigm in time series forecasting.

Nevertheless, the predominant use of MSE loss in neural network-based forecasting introduces fundamental constraints: the regression framework provides no inherent uncertainty quantification, and the quadratic loss term amplifies the influence of anomalous observations.

Researchers have developed specialized approaches that each target specific aspects of the problem in regression. For uncertainty quantification, probabilistic methods like Gaussian Processes (Seeger 2004) offer principled Bayesian uncertainty estimates but struggle with computational scalability, while quantile regression (Koenker and Hallock 2001) provides prediction intervals but may violate natural ordering constraints. Deep generative models (Kingma and Welling 2013) can capture complex distributions but require substantial training data and careful tuning. On the robustness front, both Huber loss (Huber 1992) and correntropy-based methods (Liu, Pokharel, and Principe 2007) can effectively mitigate outlier sensitivity while lacking probabilistic uncertainty quantification. The adaptive weighting scheme (Kendall, Gal, and Cipolla 2018), despite enabling dynamic sample weighting, requires joint optimization of multiple interacting hyperparameters that critically determine its performance. However, no existing method simultaneously addresses uncertainty quantification and robustness.

To this end, we propose OCE-TS as an integrated solution combining probabilistic uncertainty quantification with robust outlier handling while preserving ordinal relationships and maintaining computational efficiency. Since time series values exhibit meaningful ordinal structure, the proposed OCE-TS method reformulates the regression task as an ordinal classification problem. Ordinal classification (Gutiérrez

et al. 2016) is a specialized machine learning task designed to handle categorical labels with inherent ordinal relationships. Its core objective is to predict discrete yet ordered categories (e.g., user ratings 1-5 stars) while preserving the sequential relationships between categories. Through ordinal classification, we obtain probabilistic outputs for each predicted value, naturally quantifying prediction uncertainty. This approach is also inspired by the concepts of stability and sample-wise reliability, which have been further explored in recent studies (Li et al. 2023; Wang et al. 2023; Wang, Qian, and Li 2020; Wang et al. 2025), helping to enhance robustness against noise and irregular patterns.

To optimize the ordinal classification model, OCE-TS uses ordinal cross-entropy (OCE) loss (Niu et al. 2016; Hu et al. 2010; Wang et al. 2022). The OCE loss modifies conventional cross-entropy through order-preserving mechanisms. By evaluating discrepancies in cumulative distribution functions (CDFs) of predicted versus true labels, it guarantees that predictions adhere to the inherent hierarchy of ordinal categories.

The main contributions of this paper are as follows:

- We propose OCE-TS, a novel approach that combines linear model with ordinal cross-entropy to solve time series value prediction problems while preserving temporal ordering constraints.
- We compare MSE (regression) and cross-entropy (classification) loss stability via influence function analysis, demonstrating that classification achieves superior stability when predicted probabilities are uniformly distributed and feature representations exhibit isotropic property;
- We verify OCE-TS’s effectiveness across multiple benchmarks, which provides empirical guarantees for a new learning paradigm for time series forecasting.

Proofs and supplementary experiments are provided in the Appendix.

Related Work

Building upon ordinal classification for time series forecasting, our work intersects with three key domains: distributional regression (already discussed in Introduction), time series forecast, and ordinal classification. We now survey the latter two research areas.

Long-term time series forecasting

Long-term time series forecasting remains highly challenging due to extended prediction horizons, error accumulation, and distribution drift. Moreover, stability and sample-wise reliability (Li et al. 2019a; Wang et al. 2022) offer useful insights for improving forecasting robustness. Recent research primarily focuses on four key directions. First, for network architecture innovation, research emphasizes enhanced long-term dependency and periodicity modeling, Transformers (Vaswani et al. 2017) and their variants (e.g., Informer (Zhou et al. 2021), Autoformer (Wu et al. 2021), FEDformer (Zhou et al. 2022), PatchTST (Nie et al. 2022)) have become predominant. Meanwhile, lightweight models (e.g., DLinear (Zeng et al. 2023), LightTS (Campos et al.

2023)) achieve comparable performance with lower computational costs in specific scenarios. Second, for time series representation learning and knowledge distillation, self-supervised learning (e.g., TS2Vec (Yue et al. 2022), TNC (Tonekaboni, Eytan, and Goldenberg 2021)) and knowledge distillation methods (e.g., TCN-Distill (Gao, Parcollet, and Lane 2021), TimeNet) are leveraged to enhance generalization capability and robustness while reducing dependence on labeled data. Third, for variable and feature hierarchical modeling, methods explicitly capture inter-variable dependencies and feature importance, primarily through cross-variable attention mechanisms (e.g., MTGNN (Wu et al. 2020), ASTGCN (Guo et al. 2019)), learnable variable selection modules, and adaptive feature transformations to improve multivariate data modeling. Finally, for large models and zero-shot inference, research explores large language models (LLMs (Gruver et al. 2023)) for contextual learning (e.g., Time-LLM (Jin et al. 2024)), enabling zero-shot forecasting and cross-domain transfer through time series tokenization and prompt tuning techniques.

Ordinal Classification Task

Ordinal classification faces challenges including strong label-order dependency, ambiguous category intervals, and limited model adaptability. Existing research primarily focuses on three directions. First, loss function design, where order-aware loss functions (e.g., threshold-based (Niu et al. 2016) and margin-based (Pitawela, Carneiro, and Chen 2025) losses) are introduced to explicitly model ordinal relationships; second, model architecture improvements, including approaches like Support Vector Ordinal Regression (SVOR) (Gu et al. 2015) and COrrrelation ALignment (CORAL) (Shi, Cao, and Raschka 2023), which address label ordering via explicit threshold partitioning and implicit ordinal encoding, while attention mechanisms (Vaswani et al. 2017) and Bayesian models (Chu, Ghahramani, and Williams 2005) demonstrate strong performance in capturing long-range dependencies and modeling uncertainty; and finally, probabilistic ordinal modeling, which adopts frameworks like ordered Probit/Logit (Liu, Wang, and Kong 2019) and cumulative link models (Gutiérrez et al. 2016) to characterize the conditional probability distribution over ordered categories, incorporating monotonicity constraints to reflect the inherent ordinal structure. Recent work on stability and reliability in multi-view learning by (Li et al. 2025) further enhances the robustness of ordinal classification methods.

Time Series Forecasting Problem

Time series forecasting aims to predict future values based on historical observations. Given a lookback window $\mathbf{X}_t = (X_t, X_{t-1}, \dots, X_{t-w+1})^\top \in \mathbb{R}^w$ of w historical observations, we predict the H -step future trajectory $\mathbf{Y} = (Y_{t+1}, \dots, Y_{t+H})^\top \in \mathbb{R}^H$ through $\hat{\mathbf{Y}} = g(\mathbf{X}_t)$, where $g : \mathbb{R}^w \rightarrow \mathbb{R}^H$ is the forecasting function. For multivariate series with M -dimensional observations $\mathbf{x}_t \in \mathbb{R}^M$, this extends to predicting $\mathbf{Y} = \{\mathbf{y}_{t+1}, \dots, \mathbf{y}_{t+H}\} \in \mathbb{R}^{H \times M}$ from input $\mathbf{X}_t = \{\mathbf{x}_t, \mathbf{x}_{t-1}, \dots, \mathbf{x}_{t-w+1}\} \in \mathbb{R}^{w \times M}$.

The forecasting quality is evaluated via:

$$\text{MSE} = \frac{1}{H} \|\mathbf{Y} - \hat{\mathbf{Y}}\|_F^2 = \frac{1}{H} \sum_{j=1}^H \|\mathbf{y}_{t+j} - \hat{\mathbf{y}}_{t+j}\|_2^2. \quad (1)$$

Minimizing MSE corresponds to fitting the conditional expectation of the true data, ensuring unbiased predictions. However, MSE only supports point estimates and fails to capture uncertainty, motivating reformulations of the forecasting task as a probability prediction problem.

Regression-to-Classification Framework

The core idea of transforming regression into classification involves shifting from predicting point estimates \hat{Y}_{t+j} through MSE minimization to learning complete predictive distributions $\pi(\hat{Y}_{t+j})$, where $\hat{Y}_{t+j} \in \mathbb{R}$ represents the original continuous predicted variable and $\pi(\hat{Y}_{t+j}) \in \mathbb{R}^K$ denotes a discrete probability distribution vector satisfying $\sum_{k=1}^K \pi_k = 1$. The probabilistic regression framework transforms continuous prediction into a distribution classification problem through three key operations.

First, the true distribution is constructed by discretizing the ground truth $Y_{t+j} \in \mathbb{R}$ into bin probabilities $p_k = F_Y(u_k) - F_Y(\ell_k)$ for $k = 1, \dots, K$, where F_Y is the empirical cumulative distribution function (CDF) and $\mathcal{B}_k = [\ell_k, u_k)$ forms a partition of the target value space.

The predictive model g_θ with parameters θ then learns to output a probability distribution $\pi(\mathbf{X}_t; \theta) = (\pi_1, \dots, \pi_K)$, where each $\pi_k = \mathbb{P}(\hat{Y}_{t+j} \in \mathcal{B}_k | \mathbf{X}_t)$ represents the predicted probability for bin k . This model is trained by minimizing the distributional discrepancy $\mathcal{L}(\theta) = D(\mathbf{p}(Y_{t+j}), \pi(\mathbf{X}_t; \theta))$ through the optimization objective $\theta^* = \arg \min_{\theta} \mathbb{E}_{\mathbf{X}_t, Y_{t+j}} [D(\mathbf{p}(Y_{t+j}), \pi(\mathbf{X}_t; \theta))]$, where D measures the divergence (e.g., cross-entropy) between the true distribution \mathbf{p} and predicted distribution π .

Finally, continuous point estimates \hat{Y}_{t+j} are recovered via $\hat{Y}_{t+j} = \mathcal{G}((v_k, \pi_k(\mathbf{X}_t; \theta^*))_{k=1}^K)$, where \mathcal{G} transforms the discrete probability distribution back to the continuous space using representative values v_k for each bin \mathcal{B}_k .

Ordinal Cross-Entropy Loss

This section presents the definition of OCE, followed by a comparative example illustrating the fundamental difference with standard cross-entropy (CE) and a novel influence function analysis that contrasts their sensitivity characteristics with MSE. See Appendix for the definition of CE.

Definition 1 (Ordinal Cross-Entropy Loss). (Hu et al. 2010) Let $Y \in \{1, \dots, K\}$ be the true class label and \hat{Y} the predicted class. Given the predicted probability distribution $\mathbf{q} = [q_1, \dots, q_K]$ where $q_k = \mathbb{P}(\hat{Y} = k)$ and the true probability distribution $\mathbf{p} = [p_1, \dots, p_K]$. We define the cumulative probabilities as: $\mathbb{P}_{\text{pred}}(\hat{Y} \leq k) = \sum_{i=1}^k q_i$, $\mathbb{P}_{\text{pred}}(\hat{Y} > k) = 1 - \mathbb{P}_{\text{pred}}(\hat{Y} \leq k)$. Let $\mathbb{P}_{\text{true}}(Y \leq k)$ represent the ground-truth cumulative distribution. For hard labels: $\mathbb{P}_{\text{true}}(Y \leq k) = \mathbb{I}\{Y \leq k\}$, where \mathbb{I} is the indicator

function. The ordinal cross-entropy loss is then:

$$\mathcal{L}_{\text{OCE}}(Y, \hat{Y}) = - \sum_{k=1}^{K-1} \left[\mathbb{P}_{\text{true}}(Y \leq k) \log \mathbb{P}_{\text{pred}}(\hat{Y} \leq k) + \mathbb{P}_{\text{true}}(Y > k) \log \mathbb{P}_{\text{pred}}(\hat{Y} > k) \right]. \quad (2)$$

Comparative Analysis of OCE and CE

Table 1 compares standard cross-entropy and ordinal cross-entropy (OCE) performance across various prediction scenarios. In Case 1, where the true distribution is $[0.8, 0.1, 0.1]$, although predicted distribution B achieves a lower CE value (0.449 vs 0.518), its OCE loss is higher (1.528 vs 1.396). This indicates that CE may underestimate the ordinal errors in predicted distribution B. Similarly, in Case 2 with a true distribution of $[0.2, 0.1, 0.7]$, while predicted distribution A shows a slightly better CE value (0.604 vs 0.624), its OCE loss (2.029) is higher, further validating the limitations of CE in evaluating ordinal relationships.

Scenario	Type	Distribution \mathbf{p}	CE	OCE
Case 1	True	[0.8, 0.1, 0.1]	–	–
	Pred A	[0.3, 0.5, 0.2]	0.518	1.396
	Pred B	[0.4, 0.1, 0.5]	0.449	1.528
Case 2	True	[0.2, 0.1, 0.7]	–	–
	Pred A	[0.6, 0.2, 0.2]	0.604	2.029
	Pred B	[0.3, 0.5, 0.2]	0.624	1.720

Table 1: Comparison of CE and OCE

Notably, the OCE loss shows greater sensitivity to deviations in class ordering between predicted and true distributions. Therefore, it is better suited for classification tasks emphasizing ordinal relationships, providing a more accurate reflection of the model’s ordering performance.

Comparative Analysis of OCE and MSE

This subsection presents a comparative influence function analysis of MSE and CE losses, focusing on their differential sensitivity to feature scaling characteristics and prediction residuals. The analysis framework applies uniformly to all cross-entropy-type losses (including both CE and OCE), as they share identical functional forms - differing only in their probability computation methods (plain softmax for CE versus cumulative probabilities for OCE).

Influence functions are widely used in robustness analysis, outlier detection, and training sample evaluation. Existing research focuses on computing IF (Koh and Liang 2017; Schioppa et al. 2022) and using them for sample selection (Pruthi et al. 2020; Basu, Pope, and Feizi 2020), whereas this paper analyzes the stability of MSE and CE losses through influence functions. We analyze and compare MSE’s and CE’s influence functions via simple linear models. We consider the standard linear regression model $y = \mathbf{x}^\top \boldsymbol{\theta} + \epsilon$, where $\mathbf{x} \in \mathbb{R}^d$ is the d -dimensional feature vector, $\boldsymbol{\theta} \in \mathbb{R}^d$ is the d -dimensional parameter vector,

$\epsilon \in \mathbb{R}$ is the scalar noise term, and $y \in \mathbb{R}$ is the scalar response. The mean squared error loss function for a data point $z = (\mathbf{x}, y)$ is given by: $L(z, \theta) = \frac{1}{2}(y - \mathbf{x}^\top \theta)^2 \in \mathbb{R}$.

Consider a K -class classification problem with a parametric softmax model. Let $\mathbf{x} \in \mathbb{R}^d$ be an input feature vector and $y \in \{1, \dots, K\}$ its corresponding class label. The model's predicted probabilities are given by:

$$p(y|\mathbf{x}; \beta) = \sigma(\mathbf{x}^\top \beta)_y = \frac{e^{\mathbf{x}^\top \beta_y}}{\sum_{k=1}^K e^{\mathbf{x}^\top \beta_k}}, \quad (3)$$

where $\beta = [\beta_1, \dots, \beta_K] \in \mathbb{R}^{d \times K}$ contains the model parameters. The cross-entropy loss for a single observation $z = (\mathbf{x}, y)$ is: $L(z, \beta) = -\sum_{k=1}^K \mathbb{I}_{y=k} \log \sigma(\mathbf{x}^\top \beta)_k$.

Influence Function (IF) measures the sensitivity of model parameters or outputs to a single training sample. Its basic form is given by:

$$\text{IF}(z) = -\mathbf{H}_\theta^{-1} \nabla_\theta \mathcal{L}(\theta, z), \quad (4)$$

where \mathbf{H}_θ denotes the Hessian matrix evaluated at the optimal parameters θ , and $\nabla_\theta \mathcal{L}$ represents the gradient of the loss function with respect to the model parameters.

The influence function for MSE can be derived as:

$$\text{IF}_{\text{MSE}}(z; \theta) = (\mathbb{E}[\mathbf{x}\mathbf{x}^\top])^{-1} \mathbf{x}(y - \mathbf{x}^\top \theta) \in \mathbb{R}^d, \quad (5)$$

which quantifies the d -dimensional effect of individual data points on parameter estimates.

The influence function for CE can be derived as:

$$\text{IF}_{\text{CE}}(z; \beta) = -(\mathbb{E}[\mathbf{x}\mathbf{x}^\top \otimes \mathbf{P}])^{-1} (\mathbf{x} \otimes (\sigma(\mathbf{x}^\top \beta) - \mathbf{e}_y)), \quad (6)$$

where $\mathbf{P} = \text{diag}(\sigma(\mathbf{x}^\top \beta)) - \sigma(\mathbf{x}^\top \beta)\sigma(\mathbf{x}^\top \beta)^\top$ is the softmax output covariance matrix ($K \times K$), $\mathbf{e}_y \in \mathbb{R}^K$ is the one-hot encoded true label, \otimes represents the Kronecker product.

As shown in Equations (5) and (6), the cross-entropy loss alleviates the influence of the covariance matrix and the residuals through transformations involving the \mathbf{P} matrix and the sigmoid function, respectively. Below, we present the specific ratio between the two effects:

Theorem 1 (Influence Function Growth Rate Comparison). *Suppose that the covariance matrix $\Sigma_X = \mathbb{E}[\mathbf{x}\mathbf{x}^\top]$ is positive definite with $\lambda_{\min}(\Sigma_X) > 0$ and the expected Softmax matrix \mathbf{P} is positive definite with $\lambda_{\min}(\mathbf{P}) > 0$. Assume the input features have finite second moments ($\mathbb{E}[\|\mathbf{x}\|_2^2] < \infty$) and the sample size exceeds the feature dimension ($n > d$). For non-degenerate predictions where the MSE residual is non-zero ($y - \mathbf{x}^\top \theta \neq 0$) and the CE probability deviation is non-trivial ($\sigma - \mathbf{e}_y \neq \mathbf{0}$), the influence function ratio $R = \|\text{IF}_{\text{CE}}\|_2 / \|\text{IF}_{\text{MSE}}\|_2$ satisfies the two-sided bound:*

$$\frac{\|\sigma - \mathbf{e}_y\|_2}{\kappa_2(\Sigma_X) \lambda_{\max}(\mathbf{P}) |y - \mathbf{x}^\top \theta|} \leq R \leq \frac{\sqrt{2} \kappa_2(\Sigma_X)}{\lambda_{\min}(\mathbf{P}) |y - \mathbf{x}^\top \theta|}, \quad (7)$$

where $\kappa_2(\Sigma_X) = \|\Sigma_X\|_2 \|\Sigma_X^{-1}\|_2$ represents the spectral condition number.

From Theorem 2, we can observe that the CE loss becomes more stable than MSE when the ratio of influence functions satisfies $R \leq 1$. This stability condition holds when the data covariance matrix is well-conditioned and model predictions avoid extreme confidence. The proof and additional discussion are provided in Appendix .

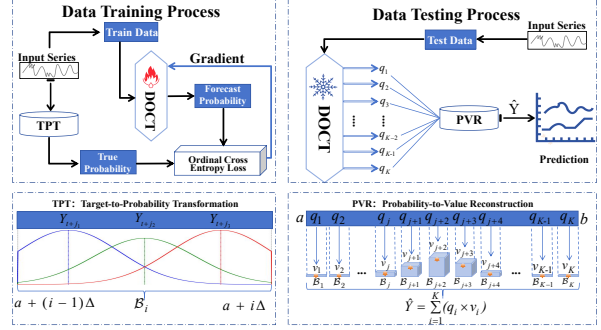


Figure 1: The Framework of Ordinal Cross-Entropy Loss-Based Time Series Forecasting (OCE-TS)

Methodology

We propose the Ordinal Cross-Entropy Time Series Forecasting (OCE-TS) method, a novel regression-to-classification framework that transforms continuous forecasting into an ordinal probability estimation problem. As shown in Figure 1, the approach consists of three key components: Target-to-Probability Transformation (TPT) that discretizes continuous values into probability distributions across ordered bins; Deep Ordinal Classifier Training using a neural architecture with ordinal cross-entropy loss to preserve the inherent ordering of bins while learning temporal patterns; and Probability-to-Value Reconstruction (PVR) that converts the predicted class probabilities back to continuous values.

Target-to-Probability Transformation

Given a true value $Y_{t+j} \in \mathbb{R}$ confined to the interval $[a, b]$, we construct its discrete probability distribution over K bins as follows. The target interval is divided into K equal-width bins, where each bin \mathcal{B}_k , $k = 1, \dots, K$ has lower and upper bounds defined by: $\mathcal{B}_k = [\ell_k, u_k)$, where $\ell_k = a + (k-1)\Delta$, $u_k = a + k\Delta$, and $\Delta = (b-a)/K$ for $k = 1, \dots, K$. Δ represents the uniform bin width, ensuring complete coverage of $[a, b]$ without overlap.

For each observation Y_{t+j} , we center a truncated Gaussian distribution at $y_c = Y_{t+j}$:

$$p(y) = \begin{cases} \frac{1}{Z\sigma\sqrt{2\pi}} \exp\left(-\frac{(y-y_c)^2}{2\sigma^2}\right) & y \in [a, b], \\ 0 & \text{otherwise.} \end{cases} \quad (8)$$

The normalization factor Z ensures unit probability mass within $[a, b]$:

$$Z = \frac{1}{2} \left[\text{erf}\left(\frac{b-y_c}{\sigma\sqrt{2}}\right) - \text{erf}\left(\frac{a-y_c}{\sigma\sqrt{2}}\right) \right]. \quad (9)$$

Here, $\text{erf}(\cdot)$ denotes the Gauss error function, and σ^2 controls the dispersion of the distribution.

The probability mass of Y_{t+j} for each bin \mathcal{B}_k is obtained

by integrating the CDF:

$$\begin{aligned} p_k^{(j)} &= \mathbb{P}(Y_{t+j} \in \mathcal{B}_k) \\ &= \frac{1}{2Z} \left[\operatorname{erf} \left(\frac{u_k - y_c}{\sigma\sqrt{2}} \right) - \operatorname{erf} \left(\frac{\ell_k - y_c}{\sigma\sqrt{2}} \right) \right]. \end{aligned} \quad (10)$$

This formulation guarantees normalization and non-negativity $\forall k: \sum_{k=1}^K p_k^{(j)} = 1, p_k^{(j)} \geq 0$.

Each observation Y_{t+j} is mapped to a K -dimensional probability vector: $\mathbf{p}^{(j)} = [p_1^{(j)}, p_2^{(j)}, \dots, p_K^{(j)}]^T$, $p_k^{(j)} = \mathbb{P}(Y_{t+j} \in \mathcal{B}_k)$, where the vector components sum to unity ($\|\mathbf{p}^{(j)}\|_1 = 1$) by construction.

Deep Ordinal Classifier Training

To obtain predictive probability distributions, this study adopts a probabilistic forecasting framework based on the Decomposition-Linear (DLinear) Model. DLinear (Zeng et al. 2023) is a time series forecasting model that employs series decomposition and multi-layer linear mapping. Given an input window $\mathbf{X}_t \in \mathbb{R}^{w \times M}$ with w time steps and M features, the model first decomposes the series into trend and residual components through moving average smoothing:

$$\mathbf{T}_t = \text{MA}_l(\mathbf{X}_t), \quad \mathbf{S}_t = \mathbf{X}_t - \mathbf{T}_t, \quad (12)$$

where $\text{MA}_l(\cdot)$ is the moving average smoothing with window size l , and \mathbf{S}_t captures residual variations. This decomposition separates temporal patterns at different scales.

The model processes each component through dedicated linear projections:

$$\tilde{\mathbf{Y}} = \mathbf{W}_t \mathbf{T}_t^\top + \mathbf{W}_s \mathbf{S}_t^\top \in \mathbb{R}^{H \times M}, \quad (13)$$

where $\mathbf{W}_t, \mathbf{W}_s \in \mathbb{R}^{H \times w}$ are learnable projection matrices. For each prediction horizon j , the scalar output \tilde{Y}_{t+j} is transformed into bin probabilities:

$$\mathbf{q} = \text{softmax}(\mathbf{W}_o \tilde{\mathbf{Y}}_{t+j} + \mathbf{b}_o), \quad (14)$$

with parameters $\mathbf{W}_o \in \mathbb{R}^{K \times M}$ and $\mathbf{b}_o \in \mathbb{R}^K$ mapping to K ordinal bins. The complete parameter set $\theta = \{\mathbf{W}_t, \mathbf{W}_s, \mathbf{W}_o, \mathbf{b}_o\}$ is optimized by minimizing:

$$\mathcal{L}(\theta) = \frac{1}{N} \frac{1}{H} \sum_{i=1}^N \sum_{j=1}^H \mathcal{L}_{\text{OCE}}(\mathbf{p}(Y_{t_i+j}), \mathbf{q}(\mathbf{X}_{t_i}; \theta)) \quad (15)$$

where \mathcal{L}_{OCE} is the ordinal cross-entropy loss (Eq. (2)), Y_{t_i+j} is the ground truth at $t_i + j$, N is the number of training windows, H the prediction horizon, and i, j index training samples and forecast steps, respectively.

The model parameters are optimized by minimizing the loss function $\mathcal{L}(\theta)$ to obtain the optimal parameters:

$$\theta^* = \arg \min_{\theta} \mathcal{L}(\theta), \quad (16)$$

after obtaining the optimal parameters θ^* , the model's prediction can be expressed as:

$$q_t = \mathbf{q}(\mathbf{X}_t; \theta^*), \quad (17)$$

where q_t is the model's prediction at time t for Y_{t+j} .

Probability-to-Value Reconstruction

The final prediction \hat{Y}_{t+j} is computed as the probability-weighted average of bin representatives $\{v_k\}_{k=1}^K$:

$$\hat{Y}_{t+j} = \mathcal{G}(\{(v_k, q_k)\}_{k=1}^K) = \sum_{k=1}^K v_k \cdot q_k, \quad (18)$$

where v_k is the predefined center of bin \mathcal{B}_k .

The above end-to-end probabilistic forecasting framework is trained using ordinal cross-entropy loss to preserve bin ordering while enabling both accurate point forecasts and uncertainty quantification.

Experimental Analysis

This section evaluates OCE-TS against five baselines on seven datasets. We analyze key factors like loss functions, parameters and distribution assumptions to validate our method. Additional experimental results are provided in the Appendix .

Experiments Settings

Dataset We conduct experiments on seven publicly available time-series datasets, including ETT (ETTh1, ETTh2, ETTm1, ETTm2), Exchange, ILL, and Weather. The detailed dataset descriptions are provided in Appendix .

Baselines. We adopt five representative models for long-term time series forecasting as our baselines, including three Transformer-based models: Autoformer (Wu et al. 2021), iTransformer (Liu et al. 2023), TimeXer (Wang et al. 2024) and TimeBridge (Liu et al. 2024), as well as one MLP-based model: DLinear (Zeng et al. 2023).

Experimental Environment The experiments are conducted on a machine equipped with an NVIDIA GeForce RTX 4060 GPU, an Intel(R) Core(TM) i7-14700F CPU, and 16 GB of RAM. The implementation requires Python 3.8.20 and PyTorch 2.0.0 compiled with CUDA 11.8 support, leveraging GPU acceleration during model training.

Evaluation Metrics The MSE and MAE are employed to evaluate model performance in time series forecasting. Lower values indicate better predictive performance. The definition of MAE is provided in Appendix .

Model Configuration and Training Details The input time series are normalized to $[-1, 1]$ or $[0, 1]$ during training and validation, and denormalized during testing for consistent metric evaluation. The support $[a, b]$ of the truncated Gaussian distribution is set to match the normalization range. Models are trained with a batch size of 32 for 15 epochs using the Adam optimizer (initial learning rate 0.005), employing dynamic learning rate adjustment based on validation performance, with an early stopping mechanism (patience=5 epochs). The input window size w is set to 336, and prediction lengths H are selected from $\{96, 192, 336, 720\}$. Details are provided in Appendix .

Comparative Results

To verify the effectiveness of the proposed method, we conduct a systematic performance comparison between OCE-TS and five mainstream models trained with the traditional MSE loss function on multiple benchmark datasets.

Dataset	H	MSE						MAE					
		Autoformer	Dlinear	Itransformer	Timexer	TimeBridge	Ours	Autoformer	Dlinear	Itransformer	Timexer	TimeBridge	Ours
ETTh1	96	0.453	0.375	0.386	0.377	0.358	0.341	0.453	0.399	0.405	0.397	0.392	0.395
	192	0.504	0.405	0.441	0.425	0.388	0.416	0.482	0.416	0.436	0.426	0.411	0.445
	336	0.505	0.439	0.487	0.457	0.401	0.491	0.484	0.443	0.458	0.441	0.419	0.491
	720	0.498	0.472	0.503	0.464	0.447	0.547	0.500	0.490	0.491	0.463	0.458	0.528
ETTh2	96	0.368	0.289	0.297	0.289	0.295	0.197	0.410	0.353	0.349	0.340	0.354	0.313
	192	0.422	0.383	0.380	0.370	0.351	0.248	0.434	0.418	0.400	0.391	0.389	0.352
	336	0.471	0.448	0.428	0.422	0.351	0.313	0.475	0.465	0.432	0.434	0.397	0.395
	720	0.474	0.605	0.427	0.429	0.388	0.379	0.484	0.551	0.445	0.445	0.436	0.435
ETTm1	96	0.481	0.299	0.334	0.309	0.297	0.195	0.463	0.343	0.368	0.352	0.353	0.308
	192	0.598	0.335	0.377	0.355	0.333	0.279	0.513	0.365	0.391	0.378	0.375	0.363
	336	0.579	0.369	0.426	0.387	0.366	0.372	0.509	0.386	0.420	0.399	0.399	0.407
	720	0.560	0.425	0.491	0.448	0.414	0.479	0.509	0.421	0.459	0.435	0.423	0.466
ETTm2	96	0.255	0.167	0.180	0.171	0.158	0.118	0.339	0.260	0.264	0.255	0.249	0.230
	192	0.281	0.224	0.250	0.238	0.215	0.167	0.340	0.303	0.309	0.300	0.291	0.279
	336	0.339	0.281	0.311	0.301	0.263	0.211	0.372	0.342	0.348	0.340	0.323	0.319
	720	0.422	0.397	0.412	0.401	0.348	0.277	0.419	0.421	0.407	0.397	0.376	0.367
Exchange	96	0.197	0.081	0.086	0.089	0.084	0.055	0.382	0.203	0.206	0.208	0.202	0.148
	192	0.300	0.157	0.177	0.196	0.189	0.107	0.369	0.293	0.299	0.313	0.310	0.224
	336	0.509	0.305	0.331	0.354	0.362	0.199	0.524	0.414	0.417	0.429	0.436	0.322
	720	1.447	0.643	0.847	0.894	0.900	0.521	0.941	0.601	0.691	0.708	0.717	0.578
ILI	24	3.483	2.215	2.695	1.971	2.055	0.570	1.287	1.081	1.703	0.868	0.890	0.458
	36	3.103	1.963	2.563	2.068	2.017	0.749	1.148	0.963	1.051	0.934	0.950	0.558
	48	2.669	2.130	2.567	1.925	1.898	1.180	1.085	1.024	1.048	0.884	0.905	0.710
	60	2.770	2.368	2.625	1.920	1.796	1.282	1.125	1.096	1.068	0.892	0.897	0.738
Weather	96	0.266	0.176	0.174	0.168	0.143	0.107	0.336	0.237	0.214	0.209	0.192	0.144
	192	0.307	0.220	0.221	0.220	0.185	0.140	0.367	0.282	0.254	0.254	0.235	0.190
	336	0.359	0.265	0.278	0.276	0.237	0.169	0.395	0.319	0.296	0.296	0.277	0.228
	720	0.419	0.323	0.358	0.353	0.307	0.225	0.428	0.362	0.347	0.347	0.330	0.283

Table 2: Comparison of Model Performances

Table 2 presents the comparative performance analysis. Given the relatively small size of the ILI dataset, its lookback window is configured as 104 timesteps with forecast horizons {24, 36, 48, 60}. Following conventional practice, other datasets adopt a fixed lookback window of 336 timesteps and forecast horizons {96, 192, 336, 720}. The experimental results show that OCE-TS achieves superior forecasting performance across most benchmark datasets.

To intuitively demonstrate the model’s fitting performance on two types of datasets, this paper visualizes the 720-step forecasting results by comparing the predicted values with the ground truth. Both the proposed method and the DLinear model use a 336-step historical sequence as input.

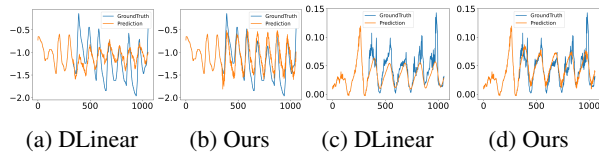


Figure 2: Model Fitting Results of DLinear and Ours

As shown in Figure 2, the first two plots forecast results on ETTm2, while the latter two show predictions for Weather. Our method tracks ground truth better than DLinear, confirming the better performance of our approach.

Table 3 shows that OCE-TS achieves high accuracy with moderate cost, balancing efficiency and performance.

models	Autoformer	Dlinear	Itransformer	Timexer	TimeBridge	Ours
ms/iter	123.3	19.3	29	17.2	21	34.9

Table 3: Per-Iteration Runtime by Model (ms)

Study of Different Probability Distributions

This section analyzes the impact of the probability distribution on the performance of the ETTh dataset. Distributions are defined in Appendix .

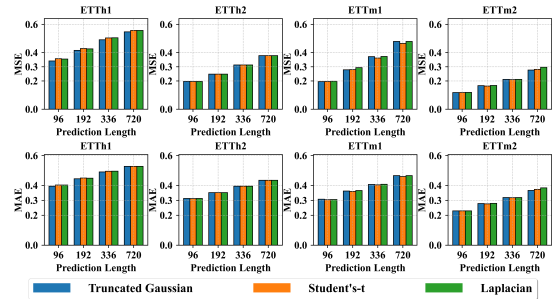


Figure 3: Distribution Comparison on ETT Datasets

As illustrated in Figure 3, the truncated Gaussian distribution achieves optimal performance on the ETTh1 dataset, demonstrating superior MSE and MAE metrics across all prediction horizons compared to both the Student’s-t distribution and Laplacian distribution, with particularly notable advantages in long-term forecasting. However,

the Student’s-t distribution exhibits better performance on ETTm2, while all three distributions show comparable results on ETTh2 and ETTm1 without statistically significant differences. Hence, the selection of an appropriate probability distribution should be carefully determined according to specific task requirements and dataset characteristics.

Lookback Window Sizes

To evaluate the impact of lookback window size on forecasting performance, this study employs multi-scale sliding windows (48 / 96 / 192 / 336 / 504 / 720 timesteps) for 720-step-ahead prediction across multiple datasets, quantitatively analyzing the correlation between historical information scale and long-term forecasting accuracy.

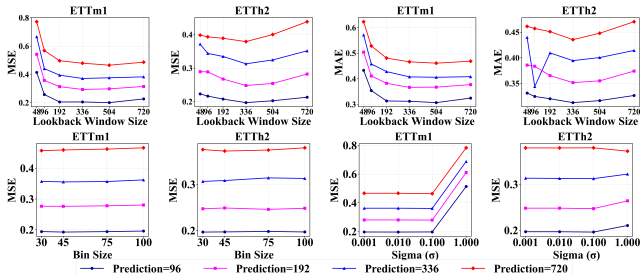


Figure 4: Lookback Window Sizes and Parameter Sensitivity

The first row of Figure 4 presents the performance of ETTm1 and ETTh2 under different lookback window lengths, the experiments show that increasing the lookback window significantly improves prediction accuracy for ETTm1 but has limited benefits for ETTh2, indicating that the optimization effect of historical information length depends on dataset characteristics. ETTm1 achieves optimal performance with ≥ 336 steps, while ETTh2 performs best at 192 steps. Therefore, the selection of the lookback window should balance accuracy and efficiency, with adjustments tailored to different datasets. Please refer to Appendix for complete experimental results and details.

Parameter Sensitivity

The OCE-TS method involves two key parameters: the number of bins (bin = K) and the standard deviation (σ). In our experimental setup, we consider bin $\in \{30, 45, 75, 100\}$ and $\sigma \in \{0.001, 0.01, 0.1, 1\}$, while keeping all other settings consistent with the baseline configuration. To systematically analyze the influence of these parameters, we examine the effect of bin by fixing $\sigma = 0.01$, and analyze the impact of σ under a fixed bin of 100. Based on these results, we provide recommendations for parameter configuration.

The second row of Figure 4 shows the variations in model performance with respect to σ values and binning parameters. The ETTm1 and ETTh2 datasets are insensitive to the number of bins but exhibit different levels of sensitivity to the standard deviation. Both datasets maintain stable performance across various bin settings; however, when $\sigma = 1$, the MSE on ETTm1 increases significantly, and ETTh2 also

experiences a performance drop. Considering both stability and accuracy, we recommend setting the number of bins to 100 and the standard deviation σ to 0.01. Please refer to Appendix for complete experimental results and details.

Comparison with CE

This section compares the performance between the OCE loss and the CE loss. See Appendix for complete experimental results and details. Experimental results in Figure 5 validate that OCE loss achieves superior metric performance (MAE / MSE) over CE loss on the Weather dataset.

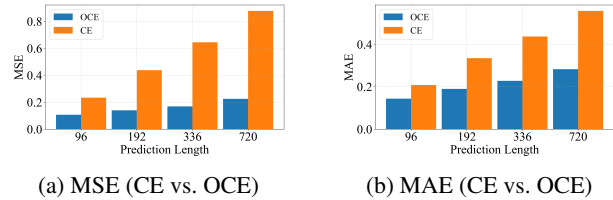


Figure 5: The Comparison between CE Loss and OCE Loss

Model Performance under Different SNRs

This experiment compares the OCE-TS method with DLinear under varying signal-to-noise ratios (SNRs) (-3 dB, 0 dB, 3 dB, 10 dB, and 20 dB), where additive Gaussian white noise is injected into inputs to evaluate robustness on the ETTm2 and Weather datasets. Please refer to Appendix for complete experimental results and details.

Dataset	-3 dB		0 dB		3 dB		10 dB		20 dB	
	MSE	Ours	MSE	Ours	MSE	Ours	MSE	Ours	MSE	Ours
ETTh2	0.440	0.275	0.431	0.274	0.425	0.273	0.420	0.277	0.420	0.280
Weather	0.342	0.227	0.339	0.225	0.338	0.224	0.337	0.223	0.338	0.224

Table 4: Comparison Under Different Noise Levels

The experimental results show that under different SNR levels, the performance of our method is superior to that of DLinear, and the impact of noise on the model’s performance is minimal, demonstrating its robustness.

Significance Analysis

To evaluate the statistical significance of performance differences among the compared algorithms, we conduct a critical difference (CD) analysis based on both MAE and MSE metrics. The x-axis of Figure 6 represents the average rankings, and algorithms connected by horizontal lines indicate no statistically significant differences. Our approach exhibits prominent superiority, with its leftmost position on the CD axis confirming statistically significant advantages over counterparts. Please refer to Appendix for more details.

Conclusion

Temporal sequence prediction plays a crucial role across various domains, yet existing models generally suffer from

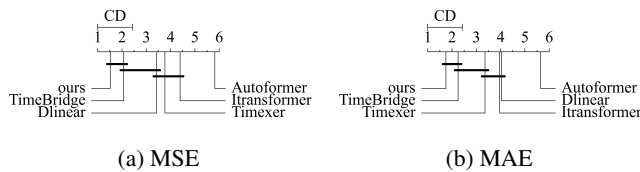


Figure 6: Critical Difference Analysis

two major limitations: insufficient uncertainty quantification and weak robustness. To address this, this paper proposes the OCE-TS framework, which synergistically integrates regression-as-classification with ordinal cross-entropy optimization to achieve more accurate predictive distribution modeling. Experiments on multiple benchmark datasets demonstrate that this approach significantly outperforms baseline models in both prediction accuracy and stability. Future work will explore more expressive distribution modeling techniques to capture complex uncertainty structures.

References

- Basu, S.; Pope, P.; and Feizi, S. 2020. Influence functions in deep learning are fragile. *arXiv preprint arXiv:2006.14651*.
- Box, G. E. P.; Jenkins, G. M.; Reinsel, G. C.; and Ljung, G. M. 2015. *Time Series Analysis: Forecasting and Control*. Hoboken, NJ: John Wiley & Sons, 5 edition.
- Campos, D.; Zhang, M.; Yang, B.; Chen, H.; Wang, S.; Xu, L.; and Li, L. 2023. LightTS: Lightweight time series classification with adaptive ensemble distillation. *Proceedings of the ACM on Management of Data*, 1(2): 1–27.
- Chu, W.; Ghahramani, Z.; and Williams, C. K. I. 2005. Gaussian processes for ordinal regression. *Journal of Machine Learning Research*, 6(7).
- Gao, Y.; Parcollet, T.; and Lane, N. D. 2021. Distilling knowledge from ensembles of acoustic models for joint CTC-attention end-to-end speech recognition. In *2021 IEEE Automatic Speech Recognition and Understanding Workshop (ASRU)*, 138–145.
- Greff, K.; Srivastava, R. K.; Koutnik, J.; Steunebrink, B. R.; and Schmidhuber, J. 2017. LSTM: A search space odyssey. *IEEE Transactions on Neural Networks and Learning Systems*, 28(10): 2222–2232.
- Gruver, N.; Finzi, M.; Qiu, S.; and Wilson, A. G. 2023. Large Language Models Are Zero-Shot Time Series Forecasters. In *Advances in Neural Information Processing Systems*, volume 36.
- Gu, B.; Sheng, V. S.; Tay, K. Y.; Romano, W.; and Li, S. 2015. Incremental Support Vector Learning for Ordinal Regression. *IEEE Transactions on Neural Networks and Learning Systems*, 26(7): 1403–1416.
- Guo, S.; Lin, Y.; Feng, N.; and et al. 2019. Attention Based Spatial-Temporal Graph Convolutional Networks for Traffic Flow Forecasting. In *Proceedings of the AAAI Conference on Artificial Intelligence*, volume 33, 922–929.
- Gutiérrez, P. A.; Perez-Ortiz, M.; Sanchez-Monedero, J.; Fernández-Navarro, F.; and Hervás-Martínez, C. 2016. Ordinal Regression Methods: Survey and Experimental Study. *IEEE Transactions on Knowledge and Data Engineering*, 28(1): 127–146.
- Hampel, F. R. 1974. The influence curve and its role in robust estimation. *Journal of the American Statistical Association*, 69(346): 383–393.
- Horn, R. A.; and Johnson, C. R. 2012. *Matrix Analysis*. Cambridge: Cambridge University Press.
- Hu, Q.; Guo, M.; Yu, D.; and Li, Q. 2010. Information Entropy for Ordinal Classification. *Science China Information Sciences*, 53(6): 1188–1200.
- Huber, P. J. 1992. Robust Estimation of a Location Parameter. In Kotz, S.; and Johnson, N. L., eds., *Breakthroughs in Statistics: Methodology and Distribution*, 492–518.
- Hyndman, R. J.; Koehler, A. B.; Ord, K.; and Snyder, R. D. 2008. *Forecasting with Exponential Smoothing: The State Space Approach*.
- Jin, M.; Wang, S.; Ma, L.; Chu, Z.; Zhang, J. Y.; Shi, X.; Chen, P.-Y.; Liang, Y.; Li, Y.-F.; Pan, S.; and Wen, Q. 2024. Time-LLM: Time Series Forecasting by Reprogramming Large Language Models. In *International Conference on Learning Representations*.
- Kendall, A.; Gal, Y.; and Cipolla, R. 2018. Multi-task Learning Using Uncertainty to Weigh Losses for Scene Geometry and Semantics. In *Proceedings of the IEEE Conference on Computer Vision and Pattern Recognition (CVPR)*, 7482–7491.
- Kingma, D. P.; and Welling, M. 2013. Auto-Encoding Variational Bayes. *arXiv preprint arXiv:1312.6114*. Online; accessed 20 December 2013.
- Koenker, R.; and Hallock, K. F. 2001. Quantile Regression. *Journal of Economic Perspectives*, 15(4): 143–156.
- Koh, P. W.; and Liang, P. 2017. Understanding black-box predictions via influence functions. In *International Conference on Machine Learning*, 1885–1894.
- Li, F.; Liu, X.; Wang, J.; and Qian, Y. 2025. MCSS: Discovering Consistently Determined Relation in Multi-view Clustering Based on Sample’s Stability. *ACM Transactions on Knowledge Discovery from Data*. Just Accepted.
- Li, F.; Qian, Y.; Wang, J.; Dang, C.; and Jing, L. 2019a. Clustering ensemble based on sample’s stability. *Artificial Intelligence*, 273: 37–55.
- Li, F.; Wang, J.; Qian, Y.; Liu, G.; and Wang, K. 2023. Fuzzy ensemble clustering based on self-coassociation and prototype propagation. *IEEE Transactions on Fuzzy Systems*, 31(10): 3610–3623.
- Li, S.; Jin, X.; Xuan, Y.; Zhou, X.; Chen, W.; Wang, Y.; and Yan, X. 2019b. Enhancing the locality and breaking the memory bottleneck of transformer on time series forecasting. *Advances in Neural Information Processing Systems*, 32.
- Lim, B.; Arik, S. O.; Loeff, N.; and Pfister, T. 2021. Temporal Fusion Transformers for Interpretable Multi-horizon Time Series Forecasting. *International Journal of Forecasting*, 37(4): 1748–1764.

- Liu, P.; Wu, B.; Hu, Y.; et al. 2024. TimeBridge: Non-Stationarity Matters for Long-term Time Series Forecasting. *arXiv preprint arXiv:2410.04442*.
- Liu, W.; Pokharel, P. P.; and Principe, J. C. 2007. Correntropy: Properties and Applications in Non-Gaussian Signal Processing. *IEEE Transactions on Signal Processing*, 55(11): 5286–5298.
- Liu, Y.; Hu, T.; Zhang, H.; Zhang, S.; Qin, Z.; Xie, Y.; Wu, Q.; Zhou, H.; and Zhang, W. 2023. iTransformer: Inverted Transformers Are Effective for Time Series Forecasting. *arXiv preprint arXiv:2310.06625*.
- Liu, Y.; Wang, F.; and Kong, A. W. K. 2019. Probabilistic deep ordinal regression based on Gaussian processes. In *Proceedings of the IEEE/CVF International Conference on Computer Vision (ICCV)*, 5301–5309.
- Nie, Y.; Nguyen, N. H.; Sinthong, P.; Wisteria, R.; Gholami, A.; and Gonzalez, J. 2022. A time series is worth 64 words: Long-term forecasting with transformers. *arXiv preprint arXiv:2211.14730*.
- Niu, Z.; Zhou, M.; Wang, L.; and Gao, Q. 2016. Ordinal Regression with Multiple Output CNN for Age Estimation. In *Proceedings of the IEEE Conference on Computer Vision and Pattern Recognition (CVPR)*, 4920–4928.
- Pitawela, D.; Carneiro, G.; and Chen, H.-T. 2025. CLOC: Contrastive Learning for Ordinal Classification with Multi-Margin N-pair Loss. In *Proceedings of the IEEE/CVF Conference on Computer Vision and Pattern Recognition (CVPR)*, 15538–15548.
- Pruthi, G.; Liu, F.; Kale, S.; et al. 2020. Estimating training data influence by tracing gradient descent. *Advances in Neural Information Processing Systems*, 33: 19920–19930.
- Schioppa, A.; Zablotzkaia, P.; Vilar, D.; Chaudhary, V.; Guzmán, F.; and Schwenk, H. 2022. Scaling Up Influence Functions. In *Proceedings of the AAAI Conference on Artificial Intelligence*, volume 36, 8179–8186.
- Seeger, M. 2004. Gaussian Processes for Machine Learning. *International Journal of Neural Systems*, 14(02): 69–106.
- Shi, X.; Cao, W.; and Raschka, S. 2023. Deep neural networks for rank-consistent ordinal regression based on conditional probabilities. *Pattern Analysis and Applications*, 26(3): 941–955.
- Taylor, S. J.; and Letham, B. 2018. Forecasting at Scale. *The American Statistician*, 72(1): 37–45.
- Tonekaboni, S.; Eytan, D.; and Goldenberg, A. 2021. Unsupervised representation learning for time series with temporal neighborhood coding. *arXiv preprint arXiv:2106.00750*.
- Vaswani, A.; Shazeer, N.; Parmar, N.; Uszkoreit, J.; Jones, L.; Gomez, A. N.; Kaiser, Ł.; and Polosukhin, I. 2017. Attention is all you need. In *Advances in Neural Information Processing Systems*, volume 30.
- Wang, J.; Li, F.; Li, J.; Hou, C.; Qian, Y.; and Liang, J. 2023. RSS-Bagging: Improving Generalization Through the Fisher Information of Training Data. *IEEE Transactions on Neural Networks and Learning Systems*, 36(2): 1974–1988.
- Wang, J.; Qian, Y.; and Li, F. 2020. Learning with mitigating random consistency from the accuracy measure. *Machine Learning*, 109(12): 2247–2281.
- Wang, J.; Qian, Y.; Li, F.; and Liu, Y. 2022. Generalization Performance of Pure Accuracy and Its Application in Selective Ensemble Learning. *IEEE Transactions on Pattern Analysis and Machine Intelligence*, 45(2): 1798–1816.
- Wang, J.; Zhang, Z.; Li, F.; Qian, Y.; and Liang, X. 2025. Stabilizing Sample Similarity in Representation via Mitigating Random Consistency. In *Proceedings of the 42nd International Conference on Machine Learning*, volume 267, 65655–65686.
- Wang, Y.; Wu, H.; Dong, J.; Liu, G.; Liu, J.; Zhao, D.; and Tian, Q. 2024. Timexer: Empowering Transformers for Time Series Forecasting with Exogenous Variables. *arXiv preprint arXiv:2402.19072*.
- Wu, H.; Xu, J.; Wang, J.; Chen, Y.; Xue, Y.; Xue, Y.; and Tian, Q. 2021. Autoformer: Decomposition transformers with auto-correlation for long-term series forecasting. *Advances in Neural Information Processing Systems*, 34: 22419–22430.
- Wu, Z.; Pan, S.; Long, G.; Jiang, J.; Chang, X.; and Zhang, C. 2020. Connecting the Dots: Multivariate Time Series Forecasting with Graph Neural Networks. In *Proceedings of the ACM SIGKDD International Conference on Knowledge Discovery & Data Mining*, 753–763.
- Yue, Z.; Wang, Y.; Duan, J.; Lin, Z.; He, Q.; Ma, Z.; Zhang, Y.; Yang, Y.; and Yu, P. S. 2022. TS2Vec: Towards universal representation of time series. In *Proceedings of the AAAI Conference on Artificial Intelligence*, volume 36, 8980–8987.
- Zeng, A.; Chen, M.; Zhang, L.; Zhou, H.; Peng, J.; Zhang, S.; and Zhang, W. 2023. Are transformers effective for time series forecasting? In *Proceedings of the AAAI Conference on Artificial Intelligence*, volume 37, 11121–11128.
- Zhou, H.; Zhang, S.; Peng, J.; Zhang, S.; Li, Z.; and Zhang, W. 2021. Informer: Beyond efficient transformer for long sequence time-series forecasting. In *Proceedings of the AAAI Conference on Artificial Intelligence*, volume 35, 11106–11115.
- Zhou, T.; Ma, Z.; Wen, Q.; Zou, Y.; Geng, X.; Li, J.; Li, H.; and Zhang, Y. 2022. Fedformer: Frequency enhanced decomposed transformer for long-term series forecasting. In *Proceedings of the International Conference on Machine Learning*, 27268–27286.

Appendix

The appendix includes:

- **A Definition and Proof.**
- **B Algorithm Framework.**
- **C More Experimental Results.**

Definition and Proof

The Definition of Cross-Entropy Loss

Definition 2 (Standard Cross-Entropy Loss (General Form)). Let $Y \in \{1, \dots, K\}$ be the true class label and \hat{Y} the predicted class. Given the predicted probability distribution $\mathbf{q} = [q_1, \dots, q_K]$ where $q_k = \mathbb{P}(\hat{Y} = k)$ and the true probability distribution $\mathbf{p} = [p_1, \dots, p_K]$, the cross-entropy loss is:

$$\mathcal{L}_{\text{CE}}(Y, \hat{Y}) = - \sum_{k=1}^K p_k \log q_k. \quad (19)$$

For hard labels (one-hot encoding):

$$p_k = \mathbb{P}_{\text{true}}(Y = k) = \begin{cases} 1 & \text{if } Y = k, \\ 0 & \text{otherwise.} \end{cases} \quad (20)$$

The cross-entropy loss simplifies to:

$$\mathcal{L}_{\text{CE}}(Y, \hat{Y}) = - \log q_Y. \quad (21)$$

where q_Y is the predicted probability for the true class.

Influence Function and Related Work

Influence functions (IF) (Hampel 1974) quantify the marginal impact of individual training samples on model parameters or predictions. First, for efficient computation, (Koh and Liang 2017) introduces stochastic Hessian inverse approximation for large models and (Schioppa et al. 2022) implements Arnoldi iteration to accelerate this for Transformers. Second, for interpretability and robustness, IFs identify influential training samples for debugging, anomaly detection, and robustness evaluation (Pruthi et al. 2020), reveal model sensitivity to input perturbations (Basu, Pope, and Feizi 2020), and aid adversarial detection and data quality assessment.

Definition 3 (Influence Function). Let T be a statistical functional mapping from a probability distribution to a real number (or vector), such as the Mean $T(P) = \mathbb{E}_P[X] = \int x dP(x)$. Let P_ϵ be the contaminated distribution with a mixture of the true distribution P and a Dirac delta distribution δ_y at y :

$$P_\epsilon = (1 - \epsilon)P + \epsilon\delta_y, \quad (22)$$

where $\epsilon \in [0, 1)$ is the contamination proportion. Intuitively, P_ϵ represents a scenario where most of the data comes from P , but a small fraction ϵ is replaced by an outlier at y .

The influence function (IF) is a fundamental tool in robust statistics that quantifies the effect of infinitesimal contamination on a statistical functional T (Koh and Liang 2017). It is defined as the directional derivative of T at P in the direction of δ_y :

$$\text{IF}(y; T, P) = \lim_{\epsilon \rightarrow 0} \frac{T(P_\epsilon) - T(P)}{\epsilon}. \quad (23)$$

If $\text{IF}(y; T, P)$ is unbounded for some y , T is non-robust (e.g., the mean). If it is bounded, T is robust (e.g., the median). IF describes how much T changes when a small fraction of data is perturbed at y .

The Influence Function of Model Parameter

In machine learning, influence function analysis quantifies the contribution of individual training samples to model parameters or predictions, revealing data importance and enhancing model interpretability. It can identify critical samples (e.g., marginal data or outliers), detect noisy or biased data, and assess model robustness.

For a model parameterized by $\theta \in \Theta$, trained via empirical risk minimization (ERM) with loss $L(\mathbf{z}, \theta)$, the empirical distribution $P_n = \frac{1}{n} \sum_{i=1}^n \delta_{\mathbf{z}_i}$. The parameter estimate $\hat{\theta}$ is obtained by minimizing the expected loss over the empirical distribution P_n :

$$\hat{\theta} = \arg \min_{\theta} \mathbb{E}_{\mathbf{z} \sim P_n} [L(\mathbf{z}, \theta)] = \arg \min_{\theta} \frac{1}{n} \sum_{i=1}^n L(\mathbf{z}_i, \theta). \quad (24)$$

To compute the influence of a new point \mathbf{z} , consider a perturbed distribution:

$$P_\epsilon = (1 - \epsilon)P_n + \epsilon\delta_{\mathbf{z}}, \quad (25)$$

where ϵ is a small weight added to the point \mathbf{z} . The new parameter estimate $\hat{\theta}_\epsilon$ minimizes:

$$\mathbb{E}_{\mathbf{z} \sim P_\epsilon} [L(\mathbf{z}, \theta)] = (1 - \epsilon)\mathbb{E}_{\mathbf{z} \sim P_n} [L(\mathbf{z}, \theta)] + \epsilon L(\mathbf{z}, \theta). \quad (26)$$

To study the sensitivity of the loss function to perturbations, we derive the derivative $\left. \frac{d\hat{\theta}_\epsilon}{d\epsilon} \right|_{\epsilon=0}$, thereby defining the influence function of θ . Analyzing the behavior at $\epsilon = 0$ (i.e., the derivative at zero perturbation) is to study the model's sensitivity to infinitesimal data perturbations. According to the first-order optimality condition and the implicit function theorem (IFT), we obtain the influence function $\text{IF}(\mathbf{z}; \hat{\theta}, P)$ is:

$$\text{IF}(\mathbf{z}; \hat{\theta}, P) = \left. \frac{d\hat{\theta}_\epsilon}{d\epsilon} \right|_{\epsilon=0} = -H_{\hat{\theta}}^{-1} \nabla_{\theta} L(\mathbf{z}, \hat{\theta}). \quad (27)$$

This quantifies how much $\hat{\theta}$ changes when an infinitesimal weight is added at \mathbf{z} .

The details of Equation (27) is obtained as follows. The Implicit Function Theorem is used to derive how $\hat{\theta}_\epsilon$ changes

with ϵ at $\epsilon = 0$. Firstly, according to the first-order optimality condition, at $\hat{\theta}_\epsilon$, the gradient of the perturbed risk is zero:

$$(1 - \epsilon)\nabla_{\theta}\mathbb{E}_{P_n}[L(\mathbf{z}, \hat{\theta}_\epsilon)] + \epsilon\nabla_{\theta}L(\mathbf{z}, \hat{\theta}_\epsilon) = 0. \quad (28)$$

Secondly, differentiate the above equality w.r.t. ϵ , then apply the chain rule and evaluate at $\epsilon = 0$, we have:

$$-\nabla_{\theta}\mathbb{E}_{P_n}[L(\mathbf{z}, \hat{\theta})] + \nabla_{\theta}L(\mathbf{z}, \hat{\theta}) \quad (29)$$

$$+ \mathbb{E}_{P_n}[\nabla_{\theta}^2 L(\mathbf{z}, \hat{\theta})] \cdot \left. \frac{d\hat{\theta}_\epsilon}{d\epsilon} \right|_{\epsilon=0} = 0. \quad (30)$$

The first term vanishes because $\hat{\theta}$ minimizes the empirical risk (gradient is zero). Finally, solve for the derivative, we have:

$$\left. \frac{d\hat{\theta}_\epsilon}{d\epsilon} \right|_{\epsilon=0} = -H_{\hat{\theta}}^{-1}\nabla_{\theta}L(\mathbf{z}, \hat{\theta}), \quad (31)$$

where $H_{\hat{\theta}} = \mathbb{E}_{P_n}[\nabla_{\theta}^2 L(\mathbf{z}, \hat{\theta})]$ is the empirical Hessian (assumed invertible).

Prerequisites for Influence Function Analysis

For matrices $\mathbf{A} \in \mathbb{R}^{m \times n}$ and $\mathbf{B} \in \mathbb{R}^{p \times q}$, their Kronecker product is defined as the block matrix (Horn and Johnson 2012):

$$\mathbf{A} \otimes \mathbf{B} = \begin{bmatrix} a_{11}\mathbf{B} & \cdots & a_{1n}\mathbf{B} \\ \vdots & \ddots & \vdots \\ a_{m1}\mathbf{B} & \cdots & a_{mn}\mathbf{B} \end{bmatrix} \in \mathbb{R}^{mp \times nq}$$

If $\Sigma_X \in \mathbb{R}^{d \times d}$ and $\mathbf{P} \in \mathbb{R}^{K \times K}$ are invertible, then:

$$(\Sigma_X \otimes \mathbf{P})^{-1} = \Sigma_X^{-1} \otimes \mathbf{P}^{-1}$$

Let $\mathbf{A} \in \mathbb{R}^{n \times n}$ be a real symmetric matrix. Its spectral norm is defined as:

$$\|\mathbf{A}\|_2 = \max_{\mathbf{x} \neq \mathbf{0}} \frac{\|\mathbf{A}\mathbf{x}\|_2}{\|\mathbf{x}\|_2} \quad (32)$$

$$= \max\{|\lambda| : \lambda \text{ is an eigenvalue of } \mathbf{A}\},$$

That is:

$$\|\mathbf{A}\|_2 = |\lambda_{\max}(\mathbf{A})|. \quad (33)$$

For arbitrary matrices \mathbf{A}, \mathbf{B} :

$$\|\mathbf{A} \otimes \mathbf{B}\|_2 = \|\mathbf{A}\|_2 \cdot \|\mathbf{B}\|_2$$

If \mathbf{X} is symmetric positive definite, the condition number of matrix $\mathbf{X} \in \mathbb{R}^{n \times n}$ measures its numerical stability:

$$\kappa_2(\mathbf{X}) := \|\mathbf{X}\|_2 \cdot \|\mathbf{X}^{-1}\|_2 = \frac{\lambda_{\max}(\mathbf{X})}{\lambda_{\min}(\mathbf{X})}.$$

Bound on Probability Residual Norm

Lemma 1. Let $\sigma \in \mathbb{R}^K$ be a probability vector from the softmax function (i.e., $\sigma_k \geq 0$, $\sum_{k=1}^K \sigma_k = 1$), and $\mathbf{e}_y \in \{0, 1\}^K$ be the one-hot encoded ground-truth label. The Euclidean norm of the probability residual satisfies:

$$\|\sigma - \mathbf{e}_y\|_2 \leq \sqrt{2}, \quad (34)$$

with equality achieved when $\sigma_y = 0$ (i.e., the model assigns zero probability to the true class).

Proof. Expand the squared norm:

$$\|\sigma - \mathbf{e}_y\|_2^2 = \sum_{k=1}^K (\sigma_k - \delta_{k,y})^2 = (1 - \sigma_y)^2 + \sum_{k \neq y} \sigma_k^2, \quad (35)$$

where $\delta_{k,y}$ is the Kronecker delta ($\delta_{k,y} = 1$ if $k = y$, else 0).

Since $\sum_{k \neq y} \sigma_k = 1 - \sigma_y$ and $\sigma_k \in [0, 1]$, the sum of squares $\sum_{k \neq y} \sigma_k^2$ is maximized when all σ_k for $k \neq y$ are equal (by convexity).

The worst case occurs when $\sigma_y = 0$ and $\sigma_k = \frac{1}{K-1}$ for $k \neq y$:

$$\|\sigma - \mathbf{e}_y\|_2^2 = (1 - 0)^2 + \sum_{k \neq y} \left(\frac{1}{K-1}\right)^2, \quad (36)$$

$$= 1 + \frac{1}{K-1} \leq 2 \quad (\forall K \geq 2). \quad (37)$$

□

IF for MSE Loss

We consider the standard linear regression model $y = \mathbf{x}^\top \theta + \epsilon$, where $\mathbf{x} \in \mathbb{R}^d$ is the d -dimensional feature vector, $\theta \in \mathbb{R}^d$ is the d -dimensional parameter vector, $\epsilon \in \mathbb{R}$ is the scalar noise term, and $y \in \mathbb{R}$ is the scalar response.

The mean squared error loss function for a data point $\mathbf{z} = (\mathbf{x}, y)$ is given by:

$$L(\mathbf{z}, \theta) = \frac{1}{2}(y - \mathbf{x}^\top \theta)^2 \in \mathbb{R} \quad (38)$$

The gradient and Hessian of the loss function take the forms:

$$\nabla_{\theta}L(\mathbf{z}, \theta) = -\mathbf{x}(y - \mathbf{x}^\top \theta) \in \mathbb{R}^d, \quad (39)$$

$$\nabla_{\theta}^2 L(\mathbf{z}, \theta) = \mathbf{x}\mathbf{x}^\top \in \mathbb{R}^{d \times d}, \quad (40)$$

where the expected Hessian $\mathbf{H}_{\theta} = \mathbb{E}[\mathbf{x}\mathbf{x}^\top] \in \mathbb{R}^{d \times d}$ corresponds to the $d \times d$ feature covariance matrix.

The influence function for MSE can be derived as:

$$\text{IF}(\mathbf{z}; \hat{\theta}) = (\mathbb{E}[\mathbf{x}\mathbf{x}^\top])^{-1} \mathbf{x}(y - \mathbf{x}^\top \hat{\theta}) \in \mathbb{R}^d \quad (41)$$

which quantifies the d -dimensional effect of individual data points on parameter estimates.

By the submultiplicative property of spectral norm, we have the upper Bound for $\|\text{IF}_{\text{MSE}}\|_2$:

$$\|\text{IF}_{\text{MSE}}\|_2 = \|\Sigma_X^{-1} \mathbf{x}(y - \mathbf{x}^\top \theta)\|_2$$

$$\leq \|\Sigma_X^{-1}\|_2 \cdot \|\mathbf{x}\|_2 \cdot |y - \mathbf{x}^\top \theta|.$$

By the definition of spectral norm, we have the lower Bound for $\|\text{IF}_{\text{MSE}}\|_2$:

$$\|\text{IF}_{\text{MSE}}\|_2 = \|\Sigma_X^{-1} \mathbf{x}(y - \mathbf{x}^\top \theta)\|_2$$

$$\geq \sigma_{\min}(\Sigma_X^{-1}) \cdot \|\mathbf{x}\|_2 \cdot |y - \mathbf{x}^\top \theta|$$

$$= \frac{\|\mathbf{x}\|_2 \cdot |y - \mathbf{x}^\top \theta|}{\|\Sigma_X\|_2} \quad (\text{since } \sigma_{\min}(\mathbf{A}^{-1}) = 1/\|\mathbf{A}\|_2).$$

The norm of the influence function $\|\text{IF}_{\text{MSE}}\|_2$ becomes large under several key conditions:

First, when samples have large prediction errors $|y - \mathbf{x}^\top \boldsymbol{\theta}| \gg 0$ (such as outliers), both the upper and lower bounds increase substantially, leading to significant growth in $\|\text{IF}_{\text{MSE}}\|_2$.

Second, the bounds scale linearly with the feature norm $\|\mathbf{x}\|_2 \gg 0$, meaning that samples with extreme feature values (known as high leverage points) exert disproportionate influence on the estimator.

Third, an ill-conditioned covariance matrix, characterized by $\|\boldsymbol{\Sigma}_X^{-1}\|_2 \gg 0$ or equivalently $\lambda_{\min}(\boldsymbol{\Sigma}_X) \approx 0$, significantly affects the influence function. This condition primarily relates to the shape of the data distribution and occurs when features exhibit near-linear dependence (collinearity). The ill-conditioning amplifies the upper bound of the influence function through the term $\|\boldsymbol{\Sigma}_X^{-1}\|_2$.

Fourth, a concentrated data distribution, indicated by $\|\boldsymbol{\Sigma}_X\|_2 \ll 1$ or equivalently $\lambda_{\max}(\boldsymbol{\Sigma}_X) \ll 1$, also increases the influence function's sensitivity. This condition reflects the overall scale of the data, showing that all features have small magnitudes (low variance). The concentration effect primarily impacts the lower bound via $\|\boldsymbol{\Sigma}_X\|_2$, making even moderate residuals more influential when the data variance is small.

These conditions interact in important ways. The ill-conditioned covariance matrix focuses on the relative scaling between features (anisotropic stretching), while the concentrated distribution concerns the absolute scale of the data (uniform shrinkage). When both conditions occur simultaneously - with $\lambda_{\min}(\boldsymbol{\Sigma}_X) \approx 0$ and $\lambda_{\max}(\boldsymbol{\Sigma}_X) \ll 1$ - their combined effect can make the estimator particularly sensitive to individual data points. Understanding these relationships helps explain why certain data characteristics lead to larger influence function values and provides insights for improving model robustness through techniques like regularization and data preprocessing.

IF for Classification

Consider a K -class classification problem with a parametric softmax model. Let $\mathbf{x} \in \mathbb{R}^d$ be an input feature vector and $y \in \{1, \dots, K\}$ its corresponding class label. The model's predicted probabilities are given by:

$$p(y|\mathbf{x}; \boldsymbol{\beta}) = \sigma(\mathbf{x}^\top \boldsymbol{\beta})_y = \frac{e^{\mathbf{x}^\top \boldsymbol{\beta}_y}}{\sum_{k=1}^K e^{\mathbf{x}^\top \boldsymbol{\beta}_k}}, \quad (42)$$

where $\boldsymbol{\beta} = [\boldsymbol{\beta}_1, \dots, \boldsymbol{\beta}_K] \in \mathbb{R}^{d \times K}$ contains the model parameters. The cross-entropy loss for a single observation $\mathbf{z} = (\mathbf{x}, y)$ is:

$$L(\mathbf{z}, \boldsymbol{\beta}) = - \sum_{k=1}^K \mathbb{I}_{y=k} \log \sigma(\mathbf{x}^\top \boldsymbol{\beta})_k, \quad (43)$$

where $\mathbb{I}_{y=k}$ denotes the indicator function that equals 1 when $y = k$ and 0 otherwise. This loss function is widely used in classification tasks due to its desirable properties, including differentiability and appropriateness for probability estimation. From Eq. (31), computing the influence function

(IF) requires both the first-order derivative (gradient) and the Hessian matrix.

Gradient Derivation The gradient of the cross-entropy loss with respect to the model parameters $\boldsymbol{\beta}$ can be computed as follows. For a single observation $\mathbf{z} = (\mathbf{x}, y)$, by the chain rule, we have:

$$\begin{aligned} \nabla_{\boldsymbol{\beta}} L(\mathbf{z}, \boldsymbol{\beta}) &= \nabla_{\boldsymbol{\beta}} [-\log \sigma(\mathbf{x}^\top \boldsymbol{\beta})_y], \\ &= -\frac{1}{\sigma(\mathbf{x}^\top \boldsymbol{\beta})_y} \nabla_{\boldsymbol{\beta}} \sigma(\mathbf{x}^\top \boldsymbol{\beta})_y, \end{aligned} \quad (44)$$

The gradient of the softmax function has two cases. For the true class y :

$$\frac{\partial \sigma(\mathbf{x}^\top \boldsymbol{\beta})_y}{\partial \boldsymbol{\beta}_y} = \sigma(\mathbf{x}^\top \boldsymbol{\beta})_y (1 - \sigma(\mathbf{x}^\top \boldsymbol{\beta})_y) \mathbf{x}, \quad (45)$$

For any other class $k \neq y$:

$$\frac{\partial \sigma(\mathbf{x}^\top \boldsymbol{\beta})_y}{\partial \boldsymbol{\beta}_k} = -\sigma(\mathbf{x}^\top \boldsymbol{\beta})_y \sigma(\mathbf{x}^\top \boldsymbol{\beta})_k \mathbf{x}, \quad (46)$$

Combining these partial derivatives, we obtain the full gradient:

$$\nabla_{\boldsymbol{\beta}} L(\mathbf{z}, \boldsymbol{\beta}) = \mathbf{x} (\sigma(\mathbf{x}^\top \boldsymbol{\beta}) - \mathbf{e}_y) \in \mathbb{R}^{d \times K}, \quad (47)$$

where \mathbf{e}_y is the one-hot vector with 1 at position y and 0 elsewhere. This compact form reveals several important properties: the gradient magnitude scales linearly with the input features \mathbf{x} ; the direction depends on the discrepancy between predictions $\sigma(\mathbf{x}^\top \boldsymbol{\beta})$ and ground truth \mathbf{e}_y ; for correctly classified examples with high confidence ($\sigma(\mathbf{x}^\top \boldsymbol{\beta})_y \approx 1$), the gradient approaches zero.

Derivation of the Hessian Matrix The Hessian matrix $H_{\boldsymbol{\beta}}$ is a second-order derivative matrix of dimension $(dK) \times (dK)$. It can be partitioned into $K \times K$ block matrices, where each block $H_{ij} \in \mathbb{R}^{d \times d}$ corresponds to the interaction between parameters $\boldsymbol{\beta}_i$ and $\boldsymbol{\beta}_j$:

$$H_{\boldsymbol{\beta}} = \begin{bmatrix} \frac{\partial^2 L}{\partial \boldsymbol{\beta}_1 \partial \boldsymbol{\beta}_1} & \cdots & \frac{\partial^2 L}{\partial \boldsymbol{\beta}_1 \partial \boldsymbol{\beta}_K} \\ \vdots & \ddots & \vdots \\ \frac{\partial^2 L}{\partial \boldsymbol{\beta}_K \partial \boldsymbol{\beta}_1} & \cdots & \frac{\partial^2 L}{\partial \boldsymbol{\beta}_K \partial \boldsymbol{\beta}_K} \end{bmatrix} \quad (48)$$

For any $i, j \in \{1, \dots, K\}$, we compute the block matrix $H_{ij} = \frac{\partial^2 L}{\partial \boldsymbol{\beta}_i \partial \boldsymbol{\beta}_j}$.

First, consider the case where $i = j = y$ (true class). The Hessian block is derived through:

$$H_{yy} = \frac{\partial}{\partial \boldsymbol{\beta}_y} [\mathbf{x} (\sigma(\mathbf{x}^\top \boldsymbol{\beta})_y - 1)], \quad (49)$$

$$= \mathbf{x} \mathbf{x}^\top \sigma(\mathbf{x}^\top \boldsymbol{\beta})_y (1 - \sigma(\mathbf{x}^\top \boldsymbol{\beta})_y), \quad (50)$$

This expression captures the curvature information specific to the correct classification decision.

Next, for the case where either $i = y, j \neq y$ or $i \neq y, j = y$, the off-diagonal blocks take the form:

$$H_{yk} = \frac{\partial}{\partial \boldsymbol{\beta}_k} [\mathbf{x} (\sigma(\mathbf{x}^\top \boldsymbol{\beta})_y)], \quad (51)$$

$$= -\mathbf{x} \mathbf{x}^\top \sigma(\mathbf{x}^\top \boldsymbol{\beta})_y \sigma(\mathbf{x}^\top \boldsymbol{\beta})_k, \quad k \neq y \quad (52)$$

These terms quantify how parameter adjustments for incorrect classes affect the true class gradient.

Finally, for cases where $i, j \neq y$ (both non-true classes), the Hessian blocks exhibit a symmetric pattern:

$$H_{ij} = \begin{cases} \mathbf{x}\mathbf{x}^\top \sigma(\mathbf{x}^\top \boldsymbol{\beta})_i (1 - \sigma(\mathbf{x}^\top \boldsymbol{\beta})_i), & i = j \\ -\mathbf{x}\mathbf{x}^\top \sigma(\mathbf{x}^\top \boldsymbol{\beta})_i \sigma(\mathbf{x}^\top \boldsymbol{\beta})_j, & i \neq j \end{cases} \quad (53)$$

revealing how incorrect classes interact with each other in parameter space.

The complete Hessian matrix admits an elegant Kronecker product representation. By defining $\mathbf{P} = \text{diag}(\sigma(\mathbf{x}^\top \boldsymbol{\beta})) - \sigma(\mathbf{x}^\top \boldsymbol{\beta})\sigma(\mathbf{x}^\top \boldsymbol{\beta})^\top \in \mathbb{R}^{K \times K}$ as the covariance matrix of softmax outputs, we obtain:

$$H_\beta = \nabla_\beta^2 L(\mathbf{z}, \boldsymbol{\beta}) = \mathbf{x}\mathbf{x}^\top \otimes \mathbf{P}, \quad (54)$$

where \otimes denotes the Kronecker product.

This compact formulation explicitly shows the Hessian's positive semi-definite nature, as both $\mathbf{x}\mathbf{x}^\top$ and the softmax covariance matrix \mathbf{P} are themselves positive semi-definite. The Kronecker structure separates the input feature interactions (through $\mathbf{x}\mathbf{x}^\top$) from the class probability relationships (through \mathbf{P}), providing insight into the loss landscape's fundamental geometry.

The expected Hessian over x is:

$$\begin{aligned} \mathbb{E}[H_\beta] \\ = \mathbb{E} [\mathbf{x}\mathbf{x}^\top \otimes (\text{diag}(\sigma(\mathbf{x}^\top \boldsymbol{\beta})) - \sigma(\mathbf{x}^\top \boldsymbol{\beta})\sigma(\mathbf{x}^\top \boldsymbol{\beta})^\top)]. \end{aligned} \quad (55)$$

IF for Cross Entropy Loss Based on the gradient and Hessian matrix of the cross-entropy loss, the complete mathematical expression of the influence function is as follows:

$$\text{IF}(\mathbf{z}; \boldsymbol{\beta}) = -\mathbf{H}_\beta^{-1} \cdot \text{vec}(\nabla_\beta L(\mathbf{z}, \boldsymbol{\beta})) \in \mathbb{R}^{dK \times 1}, \quad (56)$$

where $\text{vec}(\boldsymbol{\alpha}) \in \mathbb{R}^{dK \times 1}$ is the matrix vectorization operation for $\boldsymbol{\alpha} \in \mathbb{R}^{d \times K}$.

The gradient term is given by:

$$\nabla_\beta L(\mathbf{z}, \boldsymbol{\beta}) = \mathbf{x} (\sigma(\mathbf{x}^\top \boldsymbol{\beta}) - \mathbf{e}_y) \in \mathbb{R}^{d \times K}, \quad (57)$$

where $\mathbf{x} \in \mathbb{R}^d$ is the input feature vector, $\sigma(\mathbf{x}^\top \boldsymbol{\beta}) \in \mathbb{R}^K$ represents the model's predicted softmax probabilities, and $\mathbf{e}_y \in \mathbb{R}^K$ is the one-hot encoding of the true label.

The Hessian inverse term takes the form:

$$\mathbf{H}_\beta^{-1} = (\mathbb{E}[\mathbf{x}\mathbf{x}^\top \otimes \mathbf{P}])^{-1}, \quad (58)$$

$$\mathbf{P} = \text{diag}(\sigma(\mathbf{x}^\top \boldsymbol{\beta})) - \sigma(\mathbf{x}^\top \boldsymbol{\beta})\sigma(\mathbf{x}^\top \boldsymbol{\beta})^\top, \quad (59)$$

Here $\mathbf{P} \in \mathbb{R}^{K \times K}$ denotes the covariance matrix of softmax outputs, and \otimes is the Kronecker product that couples the feature space ($d \times d$) with the class space ($K \times K$).

By using the submultiplicative property of spectral norm and Kronecker product norm, we have the upper Bound for

$\|\text{IF}_{\text{CE}}\|_2$:

$$\|\text{IF}_{\text{CE}}\|_2 = \|(\mathbb{E}[\mathbf{x}\mathbf{x}^\top \otimes \mathbf{P}])^{-1}(\mathbf{x} \otimes (\boldsymbol{\sigma} - \mathbf{e}_y))\|_2 \quad (60)$$

$$\leq \|(\mathbb{E}[\mathbf{x}\mathbf{x}^\top \otimes \mathbf{P}])^{-1}\|_2 \cdot \|\mathbf{x} \otimes (\boldsymbol{\sigma} - \mathbf{e}_y)\|_2 \quad (61)$$

$$= \|(\boldsymbol{\Sigma}_X \otimes \mathbf{P})^{-1}\|_2 \cdot \|\mathbf{x}\|_2 \cdot \|\boldsymbol{\sigma} - \mathbf{e}_y\|_2 \quad (62)$$

$$= \|\boldsymbol{\Sigma}_X^{-1} \otimes \mathbf{P}^{-1}\|_2 \cdot \|\mathbf{x}\|_2 \cdot \|\boldsymbol{\sigma} - \mathbf{e}_y\|_2 \quad (63)$$

$$= \|\boldsymbol{\Sigma}_X^{-1}\|_2 \cdot \|\mathbf{P}^{-1}\|_2 \cdot \|\mathbf{x}\|_2 \cdot \|\boldsymbol{\sigma} - \mathbf{e}_y\|_2 \quad (64)$$

$$= \frac{1}{\lambda_{\min}(\boldsymbol{\Sigma}_X)} \cdot \frac{1}{\lambda_{\min}(\mathbf{P})} \cdot \|\mathbf{x}\|_2 \cdot \|\boldsymbol{\sigma} - \mathbf{e}_y\|_2 \quad (65)$$

$$\leq \frac{\sqrt{2}\|\mathbf{x}\|_2}{\lambda_{\min}(\boldsymbol{\Sigma}_X)\lambda_{\min}(\mathbf{P})} \quad (\text{since } \|\boldsymbol{\sigma} - \mathbf{e}_y\|_2 \leq \sqrt{2}). \quad (66)$$

By the Matrix-vector norm inequality, we have the lower Bound for $\|\text{IF}_{\text{CE}}\|_2$:

$$\|\text{IF}_{\text{CE}}\|_2 = \|(\boldsymbol{\Sigma}_X \otimes \mathbf{P})^{-1}(\mathbf{x} \otimes (\boldsymbol{\sigma} - \mathbf{e}_y))\|_2 \quad (67)$$

$$\geq \frac{\|\mathbf{x} \otimes (\boldsymbol{\sigma} - \mathbf{e}_y)\|_2}{\|\boldsymbol{\Sigma}_X \otimes \mathbf{P}\|_2} \quad (68)$$

$$= \frac{\|\mathbf{x}\|_2 \cdot \|\boldsymbol{\sigma} - \mathbf{e}_y\|_2}{\|\boldsymbol{\Sigma}_X\|_2 \cdot \|\mathbf{P}\|_2}. \quad (69)$$

The norm of the influence function $\|\text{IF}_{\text{CE}}\|_2$ becomes large under several key conditions:

First, the influence scales linearly with the input feature norm $\|\mathbf{x}\|_2$, indicating that samples with larger feature magnitudes (high-leverage points) disproportionately affect the model parameters.

Second, both bounds depend critically on the spectrum of $\boldsymbol{\Sigma}_X$. The upper bound grows as $\lambda_{\min}(\boldsymbol{\Sigma}_X)^{-1}$, showing extreme sensitivity to collinear features ($\lambda_{\min} \approx 0$), while the lower bound shrinks with $\|\boldsymbol{\Sigma}_X\|_2$, revealing that concentrated data distributions (small eigenvalues) make all samples more influential. This highlights the importance of regularization for stable influence patterns.

Third, the term $\lambda_{\min}(\mathbf{P})^{-1}$ creates a prediction confidence paradox: samples where the model is overconfident ($\lambda_{\min}(\mathbf{P}) \rightarrow 0$) can have unbounded influence. This reveals a fundamental tension in softmax models - high confidence predictions may indicate vulnerable decision boundaries overly sensitive to specific training points, regardless of prediction accuracy.

Influence Function Growth Rate Comparison

Theorem 2. Suppose that the covariance matrix $\boldsymbol{\Sigma}_X = \mathbb{E}[\mathbf{x}\mathbf{x}^\top]$ is positive definite with $\lambda_{\min}(\boldsymbol{\Sigma}_X) > 0$ and the expected Softmax matrix \mathbf{P} is positive definite with $\lambda_{\min}(\mathbf{P}) > 0$. Assume the input features have finite second moments ($\mathbb{E}[\|\mathbf{x}\|_2^2] < \infty$) and the sample size exceeds the feature dimension ($n > d$). For non-degenerate predictions where the MSE residual is non-zero ($y - \mathbf{x}^\top \boldsymbol{\theta} \neq 0$) and the CE probability deviation is non-trivial ($\boldsymbol{\sigma} - \mathbf{e}_y \neq \mathbf{0}$), the influence function ratio $R = \|\text{IF}_{\text{CE}}\|_2 / \|\text{IF}_{\text{MSE}}\|_2$ satisfies the two-sided bound:

$$\frac{\|\boldsymbol{\sigma} - \mathbf{e}_y\|_2}{\kappa_2(\boldsymbol{\Sigma}_X)\lambda_{\max}(\mathbf{P})|y - \mathbf{x}^\top \boldsymbol{\theta}|} \leq R \leq \frac{\sqrt{2}\kappa_2(\boldsymbol{\Sigma}_X)}{\lambda_{\min}(\mathbf{P})|y - \mathbf{x}^\top \boldsymbol{\theta}|} \quad (70)$$

where $\kappa_2(\Sigma_X) = \|\Sigma_X\|_2 \|\Sigma_X^{-1}\|_2$ represents the spectral condition number.

Proof. Using the above bounds, we derive the ratio $R = \frac{\|\text{IF}_{\text{CE}}\|_2}{\|\text{IF}_{\text{MSE}}\|_2}$: The upper bound is:

$$\begin{aligned} R &\leq \frac{\frac{\sqrt{2}\|\mathbf{x}\|_2}{\lambda_{\min}(\Sigma_X)\lambda_{\min}(\mathbf{P})}}{\frac{\|\mathbf{x}\|_2\|y - \mathbf{x}^\top\boldsymbol{\theta}\|}{\|\Sigma_X\|_2}} = \frac{\sqrt{2}\|\Sigma_X\|_2}{\lambda_{\min}(\Sigma_X)\lambda_{\min}(\mathbf{P})|y - \mathbf{x}^\top\boldsymbol{\theta}|} \\ &= \frac{\sqrt{2}\kappa_2(\Sigma_X)}{\lambda_{\min}(\mathbf{P})|y - \mathbf{x}^\top\boldsymbol{\theta}|} \quad (\text{where } \kappa_2(\Sigma_X) = \frac{\|\Sigma_X\|_2}{\lambda_{\min}(\Sigma_X)}) \end{aligned}$$

and the lower bound is:

$$\begin{aligned} R &\geq \frac{\frac{\|\mathbf{x}\|_2\|\boldsymbol{\sigma} - \mathbf{e}_y\|_2}{\|\Sigma_X\|_2\|\mathbf{P}\|_2}}{\|\Sigma_X^{-1}\|_2 \cdot \|\mathbf{x}\|_2 \cdot |y - \mathbf{x}^\top\boldsymbol{\theta}|} \\ &= \frac{\|\boldsymbol{\sigma} - \mathbf{e}_y\|_2}{\|\Sigma_X\|_2 \cdot \|\Sigma_X^{-1}\|_2 \cdot \|\mathbf{P}\|_2 \cdot |y - \mathbf{x}^\top\boldsymbol{\theta}|} \\ &= \frac{\|\boldsymbol{\sigma} - \mathbf{e}_y\|_2}{\kappa_2(\Sigma_X)\lambda_{\max}(\mathbf{P})|y - \mathbf{x}^\top\boldsymbol{\theta}|}. \end{aligned}$$

Thus we obtain the final combined bounds:

$$\frac{\|\boldsymbol{\sigma} - \mathbf{e}_y\|_2}{\kappa_2(\Sigma_X)\lambda_{\max}(\mathbf{P})|y - \mathbf{x}^\top\boldsymbol{\theta}|} \leq R \leq \frac{\sqrt{2}\kappa_2(\Sigma_X)}{\lambda_{\min}(\mathbf{P})|y - \mathbf{x}^\top\boldsymbol{\theta}|}. \quad \square$$

The cross-entropy (CE) loss becomes more stable than mean squared error (MSE) when the ratio of influence functions satisfies $R \leq 1$. This stability condition holds when the data covariance matrix is well-conditioned and model predictions avoid extreme confidence. Mathematically, the critical threshold occurs when the spectral condition number $\kappa_2(\Sigma_X)$ is bounded by:

$$\kappa_2(\Sigma_X) \leq \frac{\lambda_{\min}(\mathbf{P})|y - \mathbf{x}^\top\boldsymbol{\theta}|}{\sqrt{2}}. \quad (71)$$

From Eq. (71), the stability of cross-entropy (CE) loss is primarily determined by two key mathematical quantities:

First, the condition number $\kappa_2(\Sigma_X)$ of the feature covariance matrix characterizes the orthogonality of the input features. When $\kappa_2(\Sigma_X) \approx 1$, the input features are approximately orthogonal (if the mean is zero and the variances are normalized, the covariance matrix is a scaled identity matrix). The gradient descent optimization process is more stable because the curvature (reflected by the eigenvalues of the Hessian matrix) is similar across different directions, allowing a single learning rate to work well for all dimensions. The sensitivity to input perturbations is reduced because the local geometry of the loss function is more uniform.

Second, the minimum eigenvalue $\lambda_{\min}(\mathbf{P})$ of the softmax covariance matrix fundamentally characterizes prediction confidence geometry - it vanishes when the model becomes overconfident in any class (If $\boldsymbol{\sigma}(\mathbf{x}^\top\boldsymbol{\beta})$ is a one-hot vector for example, $\boldsymbol{\sigma}(\mathbf{x}^\top\boldsymbol{\beta}) = \mathbf{e}_k$, a direct calculation shows that $\mathbf{P} = 0$, and thus $\lambda_{\min}(\mathbf{P}) = 0$), indicating degenerate curvature in the loss landscape. This spectral property directly controls influence function stability, with smaller $\lambda_{\min}(\mathbf{P})$ values amplifying sample influence.

Algorithm Framework

The OCE-TS Architecture

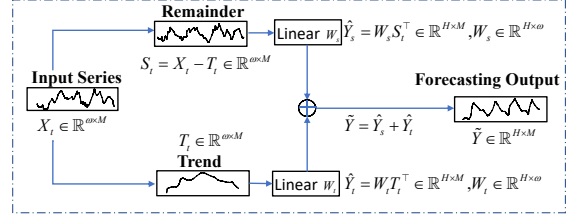


Figure 7: The framework of the DLinear model

The OCE-TS algorithm is developed by modifying the the Decomposition-Linear (DLinear) Model. As shown in Figure 7, the DLinear (Zeng et al. 2023) framework employs a decomposition-based approach for time series forecasting by separating the input series into trend and residual components. The procedure of DLinear is outlined as follows: Given an input lookback window $\mathbf{X}_t = \{\mathbf{x}_t, \mathbf{x}_{t-1}, \dots, \mathbf{x}_{t-w+1}\} \in \mathbb{R}^{w \times M}$ consisting of w historical observations with M features, the model first decomposes the series into a trend component $\mathbf{T}_t = \text{MA}_k(\mathbf{X}_t)$, obtained via moving average smoothing with window size k , and a residual component $\mathbf{S}_t = \mathbf{X}_t - \mathbf{T}_t$. The trend is then processed through weights $\mathbf{W}_t \in \mathbb{R}^{H \times w}$ to capture global patterns, yielding predictions $\hat{\mathbf{Y}}_t = \mathbf{W}_t \mathbf{T}_t^\top$, while the residuals are transformed via weights $\mathbf{W}_s \in \mathbb{R}^{H \times w}$ to model local fluctuations, producing $\hat{\mathbf{Y}}_s = \mathbf{W}_s \mathbf{S}_t^\top$.

The final H -step prediction $\tilde{\mathbf{Y}} \in \mathbb{R}^{H \times M}$ combines both components:

$$\tilde{\mathbf{Y}} = \underbrace{\mathbf{W}_t \cdot \text{MA}_k(\mathbf{X}_t^\top)}_{\text{Trend}} + \underbrace{\mathbf{W}_s \cdot (\mathbf{X}_t^\top - \text{MA}_k(\mathbf{X}_t^\top))}_{\text{Residual}}. \quad (72)$$

This dual-component design enables DLinear to simultaneously capture long-term trends and short-term variations while maintaining computational efficiency through linear operations.

At the output layer of the DLinear model, we introduce a softmax classification head to convert the predicted values $\tilde{\mathbf{Y}}$ into a probability distribution $\mathbf{q} \in \mathbb{R}^K$ over K ordinal categories. For ground truth values \mathbf{Y} , we generate target probability distributions $\mathbf{p} \in \mathbb{R}^K$ using a Truncated Gaussian Distribution. The model parameters (including trend weights \mathbf{W}_t and residual weights \mathbf{W}_s) are trained end-to-end by optimizing the OCE loss function, which minimizes the divergence between predicted probabilities \mathbf{q} and target distributions \mathbf{p} .

The OCE-TS Algorithm

The framework of our proposed OCE-TS algorithm is presented in Algorithm 1.

Algorithm 1: OCE-TS Framework

Require: $\mathcal{D} = \{\mathbf{X}_{t_i}, Y_{t_i+j}\}$: Training dataset
Require: K : Number of bins
Require: $[a, b]$: Target value range
Require: σ : Standard deviation of truncated Gaussian
Require: w : Input window size
Require: H : Prediction horizon
Require: η : Learning rate
Require: B : Batch size
Ensure: Trained model parameters θ^*

- 1: **1. Target-to-Probability Transformation**
- 2: **for** each observation $Y_{t_i+j} \in \mathcal{D}$ **do**
- 3: Partition $[a, b]$ into K bins $\mathcal{B}_k = [\ell_k, u_k)$ where $\ell_k = a + (k-1)\Delta$, $u_k = a + k\Delta$, $\Delta = \frac{b-a}{K}$
- 4: Compute $p_k^{(j)} = \frac{1}{2Z} \left[\operatorname{erf} \left(\frac{u_k - Y_{t_i+j}}{\sigma\sqrt{2}} \right) - \operatorname{erf} \left(\frac{\ell_k - Y_{t_i+j}}{\sigma\sqrt{2}} \right) \right]$ $=$
- 5: Store $\mathbf{p}^{(j)} \leftarrow [p_1^{(j)}, \dots, p_K^{(j)}]^\top$
- 6: **end for**
- 7: **2. Batch Training**
- 8: **repeat**
- 9: Sample batch $\{(\mathbf{X}_{t_i}^{(b)}, \mathbf{Y}_{t_i+j}^{(b)})\}_{b=1}^B$ from \mathcal{D}
- 10: **for** $b \leftarrow 1$ **to** B **do**
- 11: $\mathbf{T}_{t_i}^{(b)} \leftarrow \frac{1}{l} \sum_{k=1}^l \mathbf{X}_{t_i-k}^{(b)}$ \triangleright MA with window size l
- 12: $\mathbf{S}_{t_i}^{(b)} \leftarrow \mathbf{X}_{t_i}^{(b)} - \mathbf{T}_{t_i}^{(b)}$ \triangleright Residual
- 13: $\tilde{\mathbf{Y}}^{(b)} \leftarrow \mathbf{W}_t(\mathbf{T}_{t_i}^{(b)})^\top + \mathbf{W}_s(\mathbf{S}_{t_i}^{(b)})^\top$ \triangleright Projection
- 14: **for** $j \leftarrow 1$ **to** H **do**
- 15: $\mathbf{q}^{(b,j)} \leftarrow \operatorname{softmax}(\mathbf{W}_o \tilde{\mathbf{Y}}_{t_i+j}^{(b)} + \mathbf{b}_o)$
- 16: $\mathcal{L}^{(b,j)} \leftarrow -\sum_{k=1}^K p_k^{(b,j)} \log q_k^{(b,j)}$
- 17: **end for**
- 18: **end for**
- 19: $\theta \leftarrow \theta - \eta \nabla_{\theta} \left(\frac{1}{BH} \sum_{b=1}^B \sum_{j=1}^H \mathcal{L}^{(b,j)} \right)$
- 20: **until** convergence
- 21: **3. Probability-to-Value Reconstruction**
- 22: **for** each test window \mathbf{X}_t **do**
- 23: **for** $j \leftarrow 1$ **to** H **do**
- 24: Compute $\hat{\mathbf{Y}}_{t+j} \leftarrow \sum_{k=1}^K v_k q_k^{(j)}$
- 25: **end for**
- 26: **end for**

More Experimental Results

Dataset Descriptions

Table 5 presents the detailed characteristics of the experimental datasets used in this study.

The Definition of Mean Absolute Error

Mean Absolute Error (MAE) is a commonly used evaluation metric in time series forecasting, mathematically defined as:

$$\text{MAE} = \frac{1}{H} \sum_{j=1}^H \|\mathbf{y}_{t+j} - \hat{\mathbf{y}}_{t+j}\|_1, \quad (73)$$

where \mathbf{y}_{t+j} and $\hat{\mathbf{y}}_{t+j}$ represent the ground truth and predicted vectors at time step $t+j$, respectively.

Dataset	Feature	Timesteps
ETTh1	7	17420
ETTh2	7	17420
ETTm1	7	69680
ETTm2	7	69680
Exchange	8	7588
ILI	7	966
Weather	21	52696

Table 5: Dataset Statistics

Data Normalization

The model processes input time series normalized to the range $[-1, 1]$ or $[0, 1]$ during training and validation (denormalized during testing), with the support $[a, b]$ of the truncated Gaussian distribution matching the normalization range.

The normalization range is determined based on the data distribution: if all values are positive, normalization is performed to $[0, 1]$; otherwise, normalization is performed to $[-1, 1]$. In this experiment, the ETT series datasets are normalized to $[0, 1]$, while other datasets are normalized to $[-1, 1]$.

Let \mathbf{x} be a time series sequence, with its minimum and maximum values denoted as \mathbf{x}_{\min} and \mathbf{x}_{\max} respectively. For normalization to the interval $[-1, 1]$, the minimum and maximum values are computed along the temporal dimension for each sample and feature. The normalization formula is:

$$\mathbf{x}_{\text{norm}} = 2 \cdot \frac{\mathbf{x} - \mathbf{x}_{\min}}{\mathbf{x}_{\max} - \mathbf{x}_{\min} + \epsilon} - 1, \quad (74)$$

where ϵ is a small constant to prevent division by zero. The corresponding denormalization formula is:

$$\mathbf{x} = \frac{\mathbf{x}_{\text{norm}} + 1}{2} \cdot (\mathbf{x}_{\max} - \mathbf{x}_{\min} + \epsilon) + \mathbf{x}_{\min}. \quad (75)$$

For normalization to the interval $[0, 1]$, the same minimum and maximum values \mathbf{x}_{\min} and \mathbf{x}_{\max} are computed along the temporal dimension for each sample and feature. The normalization is performed as:

$$\mathbf{x}_{\text{norm}} = \frac{\mathbf{x} - \mathbf{x}_{\min}}{\mathbf{x}_{\max} - \mathbf{x}_{\min} + \epsilon}. \quad (76)$$

The denormalization formula is:

$$\mathbf{x} = \mathbf{x}_{\text{norm}} \times (\mathbf{x}_{\max} - \mathbf{x}_{\min} + \epsilon) + \mathbf{x}_{\min}. \quad (77)$$

The normalization operation for $\mathbf{X}_{t_i}^{(b)}$ and $\mathbf{Y}_{t_i+j}^{(b)}$ directly use the maximum and minimum values of the input sequence $\mathbf{X}_{t_i}^{(b)}$ and $\mathbf{Y}_{t_i+j}^{(b)}$, respectively. For denormalization, the predicted values $\hat{\mathbf{Y}}_{t+j}$ strictly employ the maximum and minimum values of the input sequence $\mathbf{X}_{t_i}^{(b)}$, thereby ensuring numerical stability during the training process.

Distributions

This section introduces two alternative probability distributions, which are incorporated into the proposed framework

to replace the truncated Gaussian distribution for validation and comparison purposes. We present the formal definitions of both distributions used in our analysis and describe the methodology for generating Figure 3.

Student's t -distribution The Student's t -distribution with ν degrees of freedom has probability density function:

$$f(y|\nu) = \frac{\Gamma\left(\frac{\nu+1}{2}\right)}{\sqrt{\nu\pi}\Gamma\left(\frac{\nu}{2}\right)} \left(1 + \frac{y^2}{\nu}\right)^{-\frac{\nu+1}{2}}, \quad (78)$$

where $\Gamma(\cdot)$ is the gamma function, $\nu > 0$ represents the degrees of freedom, and the distribution converges to the standard normal distribution as $\nu \rightarrow \infty$.

For the observation $Y_{t+j} = y_c$, we model the predictive distribution using a truncated t -distribution with $\nu = 5$ degrees of freedom, centered on the interval $[a, b]$:

$$p(y) = \begin{cases} \frac{1}{Z\sigma} f\left(\frac{y-y_c}{\sigma} \middle| 5\right), & x \in [a, b] \\ 0, & \text{otherwise} \end{cases}, \quad (79)$$

The choice of $\nu = 5$ provides moderate tail heaviness, allowing the model to better handle outliers while retaining a near-Gaussian shape. Here, $f(\cdot|\nu)$ denotes the PDF of a standard t -distribution with $\nu = 5$ degrees of freedom, and σ is the scale parameter.

The normalization constant Z ensures that the total probability integrates to one over the interval $[a, b]$. It is computed by the difference of cumulative distribution function (CDF) values:

$$Z = F_5\left(\frac{b-y_c}{\sigma}\right) - F_5\left(\frac{a-y_c}{\sigma}\right), \quad (80)$$

where $F_5(\cdot)$ is the CDF of the standard t -distribution with 5 degrees of freedom.

For discretized bins $[\ell_k, u_k]$ within $[a, b]$, the probability mass assigned to the k -th bin at horizon j is given by:

$$p_k^{(j)} = \frac{1}{Z} \left[F_5\left(\frac{u_k-y_c}{\sigma}\right) - F_5\left(\frac{\ell_k-y_c}{\sigma}\right) \right]. \quad (81)$$

In evaluating the impact of different distributions on experimental performance, when the Gaussian distribution is replaced with the Student's t -distribution, the equations in the main text, namely Eqs. (8), (9), and (11), are respectively replaced by Equations (79), (80), and (81).

Laplace Distribution The Laplace distribution (double exponential) with location μ and scale $\lambda > 0$ has the probability density function:

$$f(y|\mu, \lambda) = \frac{1}{2\lambda} \exp\left(-\frac{|y-\mu|}{\lambda}\right), \quad (82)$$

where $\mu \in \mathbb{R}$ is the location parameter and λ controls the spread. The distribution is symmetric about μ and has heavier tails than the normal distribution. The scale parameter λ relates to the standard deviation σ through:

$$\sigma = \sqrt{2}\lambda \quad \text{or equivalently} \quad \lambda = \frac{\sigma}{\sqrt{2}}. \quad (83)$$

To ensure a fair comparison across distributional assumptions, we align the variance of the Laplace distribution with that of the Gaussian. Specifically, we set

$$\lambda = \frac{\sigma}{\sqrt{2}} \approx 0.00707, \quad (84)$$

given $\sigma = 0.01$, so that both distributions share the same scale and yield consistent predictive behavior.

For the observation $Y_{t+j} = y_c$, we model the predictive distribution using a truncated Laplace distribution with scale parameter λ , centered on the interval $[a, b]$:

$$p(y) = \begin{cases} \frac{1}{Z\lambda} f\left(\frac{y-y_c}{\lambda} \middle| \mu = 0\right), & \in [a, b] \\ 0, & \text{otherwise} \end{cases}, \quad (85)$$

Here, $f(\cdot|\mu)$ denotes the probability density function (PDF) of a Laplace distribution with location parameter $\mu = 0$.

The normalization constant Z ensures the total probability integrates to one over $[a, b]$, computed by the difference of the Laplace cumulative distribution function (CDF) values:

$$Z = F_{\text{Laplace}}\left(\frac{b-y_c}{\lambda}\right) - F_{\text{Laplace}}\left(\frac{a-y_c}{\lambda}\right), \quad (86)$$

where $F_{\text{Laplace}}(\cdot)$ is the CDF of the standard Laplace distribution.

For discretized bins $[\ell_k, u_k]$ within $[a, b]$, the probability mass assigned to the k -th bin at horizon j is given by:

$$p_k^{(j)} = \frac{1}{Z} \left[F_{\text{Laplace}}\left(\frac{u_k-y_c}{\lambda}\right) - F_{\text{Laplace}}\left(\frac{\ell_k-y_c}{\lambda}\right) \right]. \quad (87)$$

To evaluate the impact of different distributions on experimental performance, when the Gaussian distribution is replaced by the Laplace distribution, the equations in the main text, namely Equations (8), (9), and (11), are respectively replaced with Equations (85), (86), and (87).

Lookback Window Sizes

Figure 8 presents the prediction performance across seven different datasets under varying lookback window sizes. For the ILI dataset, prediction lengths are set as $\{24, 36, 48, 60\}$ and lookback window sizes are selected from $\{52, 78, 104, 130, 156, 208\}$. For the remaining datasets, prediction lengths are chosen from $\{96, 192, 336, 720\}$, with lookback windows drawn from $\{48, 96, 192, 336, 504, 720\}$.

The experimental results demonstrate that the impact of different lookback window sizes on prediction performance exhibits significant dataset dependency. For most datasets including ETT and Weather, increasing the lookback window effectively reduces prediction errors (MSE / MAE), indicating that longer historical data helps capture long-term dependencies, though with diminishing returns - for instance, the ETTh series shows limited improvement when the window exceeds 336. In contrast, more volatile datasets like Exchange and period-sensitive datasets like ILI show greater sensitivity to window size, requiring case-specific optimization. Furthermore, short-term predictions (e.g., 96 / 192) generally outperform long-term forecasts (e.g., 336

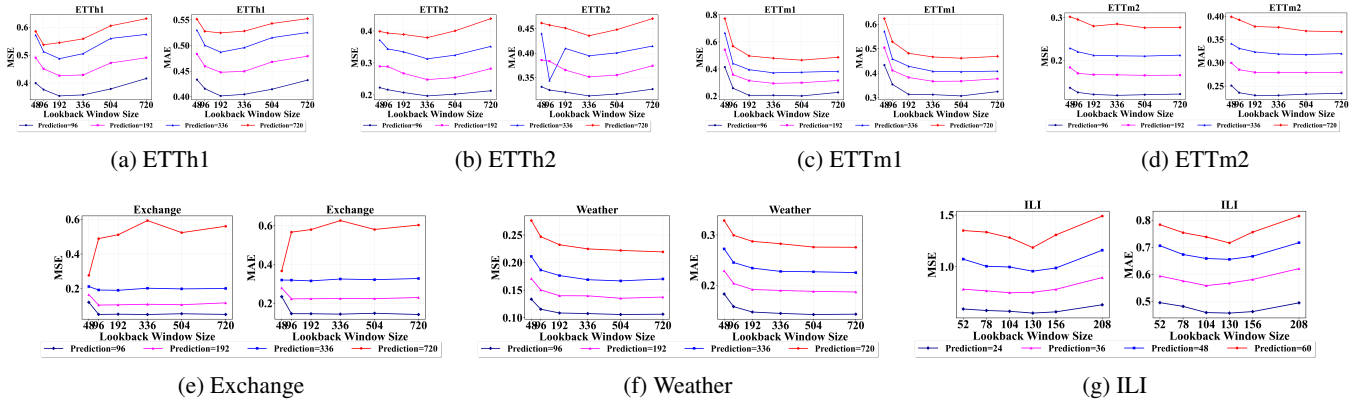


Figure 8: MSE and MAE results on seven datasets: ETTh1, ETTh2, ETTm1, ETTm2, Exchange, Weather, and ILI.

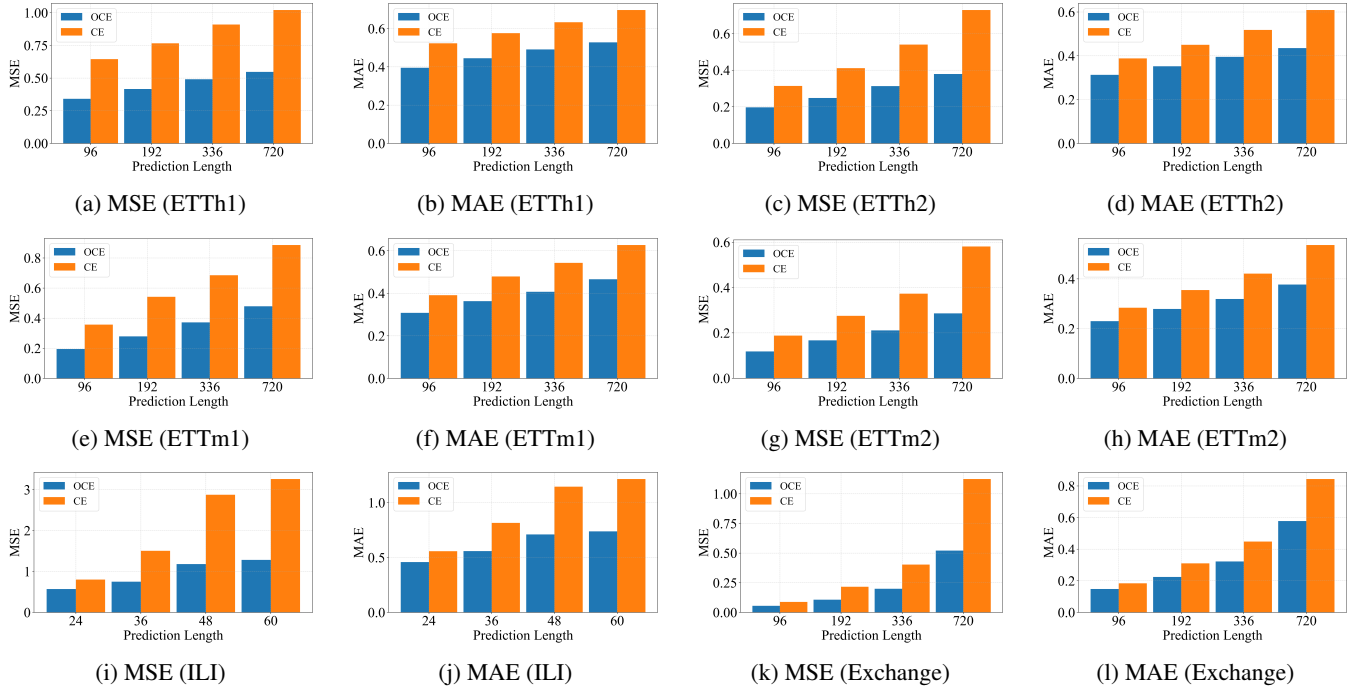


Figure 9: Performance Comparison Between CE and OCE Loss Functions Across Six Datasets.

Dataset	Pred	-3dB				0dB				3dB				10dB				20dB			
		DLinear		Ours		DLinear		Ours		DLinear		Ours		DLinear		Ours		DLinear		Ours	
		MSE	MAE	MSE	MAE																
ETTh2	96	0.186	0.284	0.117	0.229	0.182	0.280	0.116	0.228	0.176	0.274	0.116	0.227	0.172	0.269	0.118	0.229	0.172	0.268	0.118	0.230
	192	0.255	0.338	0.163	0.278	0.246	0.328	0.162	0.277	0.241	0.323	0.162	0.276	0.235	0.317	0.163	0.277	0.235	0.316	0.164	0.277
	336	0.285	0.345	0.207	0.318	0.280	0.340	0.206	0.317	0.277	0.337	0.206	0.317	0.276	0.336	0.207	0.317	0.277	0.337	0.209	0.318
	720	0.440	0.453	0.275	0.373	0.431	0.446	0.274	0.372	0.425	0.442	0.273	0.371	0.420	0.438	0.277	0.372	0.420	0.437	0.280	0.374
Weather	96	0.186	0.253	0.109	0.149	0.181	0.247	0.109	0.147	0.178	0.242	0.108	0.145	0.176	0.237	0.107	0.145	0.175	0.236	0.107	0.144
	192	0.224	0.285	0.139	0.193	0.226	0.291	0.138	0.191	0.224	0.288	0.137	0.190	0.221	0.284	0.136	0.189	0.221	0.283	0.136	0.189
	336	0.272	0.330	0.173	0.232	0.269	0.326	0.171	0.230	0.267	0.324	0.170	0.229	0.266	0.321	0.168	0.228	0.266	0.321	0.169	0.228
	720	0.342	0.388	0.227	0.283	0.339	0.384	0.225	0.281	0.338	0.382	0.224	0.280	0.337	0.381	0.223	0.279	0.338	0.381	0.224	0.280

Table 6: MSE and MAE Comparison of DLinear and OCE-TS Under Different Noise Levels

/ 720). While expanding the lookback window typically enhances performance, it necessitates balancing computational costs against diminishing returns. We recommend using medium-sized windows (192 / 336) as a baseline for specific data characteristics, followed by experimental fine-tuning. These findings provide guidance for balancing historical information utilization in time series forecasting.

Parameter Sensitivity

The OCE-TS method incorporates two critical hyperparameters: the number of discrete bins (*bin*) and standard deviation (σ). Our comprehensive parameter sensitivity analysis examines the complete parameter space defined by $bin \in \{30, 45, 75, 100\}$ and $\sigma \in \{0.001, 0.01, 0.1, 1\}$, with all other experimental configurations held constant relative to the baseline model. To precisely evaluate individual parameter effects, we implement a controlled variable approach consisting of two analytical phases: (1) performance impact assessment of *bin* variations with fixed $\sigma = 0.01$, followed by (2) regulatory effect analysis of σ adjustments with fixed $bin = 100$. This systematic parameter investigation is conducted on the ETT time series dataset collection, employing both MSE and MAE as primary evaluation metrics.

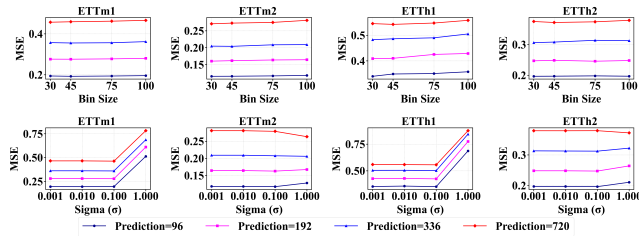


Figure 10: Comparison of MSE performance across different bin sizes (top row) and sigma values (bottom row) for four datasets. The plots show results for prediction lengths 96, 192, 336, and 720.

Experimental results demonstrate that the adjustment of bin size has relatively limited impact on model performance, whereas the value of standard deviation (σ) significantly affects the prediction results. The default parameter setting of $bin = 75$ and $\sigma = 0.01$ achieves consistently strong performance across most datasets and prediction lengths. It is recommended to first fix $\sigma = 0.01$ and tune *bin* within the range [75, 100]. For the ETTh series or long-term forecasting tasks, increasing *bin* to 100 may yield better results. If performance fluctuations are observed, further fine-tuning σ within the range [0.005, 0.05] is suggested to enhance stability and robustness.

Comparison of Loss Functions

To provide a more comprehensive comparison between the CE and OCE loss functions, Figure 9 presents the complete visualization results across six benchmark datasets under both MSE and MAE metrics.

The experimental results demonstrate that the proposed OCE loss function (marked in blue) significantly outperforms the baseline CE loss function (marked in yellow)

on both MSE and MAE metrics. This performance advantage shows consistent improvement across all benchmark datasets, validating the superiority of the OCE loss function for time series forecasting tasks.

Model Performance under Different SNRs

To assess model robustness under noisy conditions, we conduct experiments by injecting additive Gaussian white noise with variance $\sigma^2 = P_{\text{signal}}/10^{\text{SNR}_{\text{dB}}/10}$ into inputs, evaluating performance across five SNR levels: -3 dB, 0 dB, 3 dB, 10 dB, and 20 dB. Here, P_{signal} is the average signal power, computed as the signal’s mean squared value, used to set the noise variance σ^2 for the target SNR. The comparative analysis between our method and DLinear is performed on both ETTm2 and Weather datasets, with comprehensive results across multiple prediction lengths summarized in Table 6 (MSE / MAE metrics).

As the noise intensity increases (i.e., lower SNR), the performance of DLinear degrades significantly. In contrast, our method maintains consistently lower MSE and MAE across all noise levels and forecast horizons, demonstrating stronger noise robustness.

Significance Analysis

The Nemenyi post-hoc test determines whether two algorithms differ significantly by comparing their average rank difference to the critical distance:

$$CD = q_\alpha \sqrt{\frac{k(k+1)}{6N}}, \quad (88)$$

where q_α is the critical value from the Studentized range distribution at significance level α , k is the number of compared algorithms, and N is the number of datasets. The performance difference is considered statistically significant when the observed rank difference exceeds CD .

The experiments compared OCE-TS with five baseline methods including Autoformer, Dlinear, and TimeBridge across seven benchmark datasets, using both MAE and MSE as evaluation metrics. We set the significance level at 0.05 for this analysis.